Title
MECHANISMS OF FOAM GENERATION IN GLASS BEAD PACKS

Authors
Ransohoff, T.C.
Radke, C.J.

Publication Date
1986-06-01

Lawrence Berkeley Laboratory
UNIVERSITY OF CALIFORNIA

EARTH SCIENCES DIVISION

Presented at the 61st Annual Meeting of the
Society of Petroleum Engineers, New Orleans, LA,
October 5-8, 1986

MECHANISMS OF FOAM GENERATION IN GLASS BEAD PACKS

T.C. Ransohoff and C.J. Radke

June 1986

Prepared for the U.S. Department of Energy under Contract DE-AC03-76SF00098

DISCLAIMER

LBL-21845

MECHANISMS OF FOAM GENERATION IN GLASS BEAD PACKS

T.C. Ransohoff[1] and C.J. Radke[1,2]

[1]Department of Chemical Engineering
University of California
Berkeley, California 94720

[2]Earth Sciences Division
Lawrence Berkeley Laboratory
University of California
Berkeley, California 94720

June 1986

This work was supported by the U.S. Department of Energy through Contract No. DE-AC03-76SF00098.

Mechanisms of Foam Generation in Glass Bead Packs

T. C. Ransohoff and C. J. Radke

University of California

Department of Chemical Engineering

Berkeley, CA 94720

ABSTRACT

The fundamental, pore-level mechanisms of foam generation are investigated in monodisperse bead packs. First, direct visual observations identify the following generation mechanisms: lamella leave behind, gas-bubble snap off, and lamella division. Then, to ascertain the relative importance of these mechanisms, quantitative experiments are pursued on the role of bead-pack permeability (bead sizes from 0.25 mm to 1 mm), gas-phase velocity (0.001 cm/s to 0.8 cm/s), gas-phase fractional flow (0.60 to 1.0), permeability variations, and surfactant type (SDBS, SDS, Chevron Chaser SD1000, and Suntech IV 1035). We discover a critical velocity, above which a "strong" foam is generated and below which only "weak" foam is formed. The snap-off mechanism is the primary mechanism responsible for the formation of the strong foam. A simple model, based on the concept of a "germination site", is developed to predict the onset of snap off at higher gas velocities. New experimental data obtained in the homogeneous glass bead packs for the critical capillary number necessary to form a strong foam are in excellent agreement with the proposed germination-site model.

INTRODUCTION

Steam flooding is a common thermal technique to recover oil which is too viscous to be displaced by standard waterflooding techniques. Two of the problems associated with steam flooding are "gravity override" and "viscous fingering." Gravity override occurs because the steam is much less dense than the oil which it is displacing, causing the steam to "ride over" the oil bank. Viscous fingering occurs because the displacing steam is much less viscous than the oil phase, causing channels or "fingers" to form. Thus, steam can bypass most of the oil.

Fried [1]suggested that these mobility problems might be ameliorated by injecting the steam in the form of a foam. Field tests have in fact demonstrated that foam can significantly increase the efficiency of a steam drive[2,3]. Foam also holds promise for CO_2 flooding and as a general mobility-control fluid.

To eliminate confusion over the meaning of "foam" in the context of this paper[4], we define foam in porous media to be a gas dispersed in an interconnected liquid comprised of stable lamellae. This definition is similar to the one presented earlier by Falls et al[5]. The important points to the definition are that the gas may exist in either continuous or discontinuous form and that the foam is not a "bulk" foam; in other words, the size of the bubbles is generally on the order of the size of the pore channels. Consequently, bubble interactions with pore walls dominate foam-flow behavior in porous media.

The success of foam as a displacing fluid is due in part to its high apparent viscosity when forced to flow through porous media[6]. Increased resistance to gas flow due to the foam reduces the rate at which gravity

override occurs and improves the mobility ratio, thus lessening the extent of viscous fingering. It has been shown by Hirasaki and Lawson[7] that the flow properties and apparent viscosity of foam in porous media are highly dependent on the texture (i.e., bubble size and bubble-size distribution) of the foam. Foam texture is, in turn, a strong function of the way in which the foam is generated. Therefore, an understanding of the generation step is crucial in predicting the efficiency of a foam drive.

Foam flooding is an excellent example of a process whose macroscopic or overall properties, such as pressure drop and displacement efficiency, depend on microscopic or pore-level events that are presently not well understood, such as gas-bubble formation and lamella breakage. For this reason, we attempt to understand the mechanisms and physical processes involved in foam generation at the pore level. First, the mechanisms of foam generation are identified in glass bead packs. Then the quantitative effects of bead size, gas velocity, and surfactant type on the foam generation process are studied.

EXPERIMENTAL METHOD

Two general types of experiments are performed. In the first set, the "visual" experiments, 16 mm movies record the primary mechanisms of foam generation in bead packs. In the second set, the "parametric" experiments, the effects of gas velocity and fractional flow, bead size, and surfactant type on the relative importance of the generation mechanisms are determined. The parametric experiments are further classified as quantitative or qualitative. Results from the quantitative experiments are tested against the theory for the critical-velocity onset of snap off; results from the qualitative experiments provide insight into the foam generation process.

All experiments are carried out in a transparent plexiglass bead pack of rectangular cross section as illustrated in Figure 1. The dimensions of the bead-filled area are 6 mm x 25 mm x 165 mm. In a pack of height h = 6 mm and when filled with beads on the order of 1 mm or smaller, gravity forces are small in relation to capillary forces (i.e., the Bond number, $Bo = \Delta\rho g R_g h/\sigma$, is less than unity). A liquid inlet, a gas inlet, a pressure transducer port, and an exit piece are attached to the bead pack. The pressure transducer (Validyne, Model DP-15) measures the gas-phase pressure drop across the entire pack.

Packing consists of plugging the inlet ports, filling the cavity approximately halfway with the liquid solution, loading and settling the glass beads, and securing the screen and exit piece to ensure a tight pack. Settling is usually aided by a Bransonic (Model 220) ultrasonic bath. Three different size glass beads (Ferro Corp., Cataphote Div.) are used, having nominal diameters of 0.25 mm, 0.5 mm, and 1 mm. The absolute permeability to water, K, and porosity, ϕ, of three representative bead packs are listed in Table 1.

Either pure water or an aqueous surfactant solution is used as the liquid phase in the foam generation experiments. The surfactants used include SDBS (sodium dodecyl benzene sulfonate, Sharpe Chem. Co., Burbank, CA), SDS (sodium dodecyl sulfate, Eastman Kodak Co., Rochester, NY), Chaser SD1000 (Chevron Chem. Co., Richmond, CA), and Suntech IV 1035 (Sun Refining and Marketing Co., Philadelphia, PA). The surface tensions of 1% (w/w) aqueous solutions of the above surfactants are measured using a Rosano surface tensiometer (Biolar Corp., North Grafton, MA) with a Wilhelmy plate. Their values are presented in Table 2.

Once the beads are packed in the selected liquid solution, gas is

injected into the model. In the quantitative experiments and in most of the qualitative experiments, the gas is nitrogen. A Brooks mass flow controller (Model 5850C with control box Model 5876) monitors and controls the gas flow. In some of the qualitative experiments, air is injected with a Harvard syringe pump (Model 975). Many experiments have a non-zero fractional flow of liquid. In the quantitative "fractional flow" experiments, liquid is injected by an Altex preparatory chromatographic pump (Model 101A) while a Harvard syringe pump is used in the qualitative experiments.

The primary visual experiments consist of two 16 mm movies produced on foam generation in homogeneous bead packs. These movies are shot at a camera speed of 50 frames per second with a Bolex H16 EBM electric movie camera resting on a Fastax tripod (Wollenstack Optical Co., Model WF 326B) using Kodak Plus-X reversal film.

In the first movie experiment, the light source is a Westinghouse 500W movie lamp, and the flow cell rests on a frosted glass platform. The f-stop is set at 4-5, and movies are taken of both the exit region and the interior of the bead pack. Magnification of approximately 5x is provided by a 20 mm extension tube attached to a 50 mm lens. The surfactant solution used is a 2% (w/w) aqueous solution of Liquinox (Alconox, Inc., New York, NY), and the nominal bead diameter is 1 mm. The gas velocity is varied from 0.04 to 0.80 cm/s in this experiment, and the fractional flow rate of gas is 1.0.

In the second movie experiment, an Ealing fiber light source illuminates the bead pack from below through a clear glass platform. The f-stop is set at 8 and the light intensity at 100% for the entire movie. A 50 mm lens is used with a 60 mm extension tube and a reversed C-mount, which provides an additional extension of approximately 20 mm; the corresponding magnification is ~20x. The surfactant solution is 0.5% (w/w) SDBS, and the bead diameter is

again 1 mm. In this experiment, liquid is injected concurrently with the gas at a fractional flow rate of 0.24; the total velocity is varied from 0.14 to 0.53 cm/s.

In the parametric experiments, the nominal bead sizes vary from 0.25 to 1 mm, the range of total velocity is from 0.001 cm/s to 0.3 cm/s, and the gas fractional flow ranges from 0.6 to 1.0. The surfactant solution used in the quantitative experiments is 1% (w/w) SDBS.

The quantitative experiments are run until either the gas forms a continuous flow path through the bead pack or a fine foam is generated inside the bead pack. In the former case, the steady gas-phase pressure drop is recorded after the continuous channel is formed and maintained. When liquid is also being injected, the gas-phase pressure drop is determined by subtracting an estimated capillary pressure term from the total pressure drop. If the pressure drop rises dramatically due to the massive generation of tiny foam bubbles, the experiment is stopped to prevent damage to the sensitive 0.5 psi transducer diaphragm. Considerable details on the experimental procedures and apparatus are available elsewhere[8].

VISUAL EXPERIMENTS

As mentioned above, the bulk of the visual observations come from two movies taken of the foam generation process in packs of 1 mm glass beads. The first movie, which was taken with a diffuse light source at low magnification levels (~5x), reveals little about pore-level mechanics. Nonetheless, some important observations emerge. At velocities below ~0.2 cm/s, large bubbles (1-5 mm in diameter with an average diameter of 2 mm) exit from the bead pack as shown in Figure 2. Closer inspection reveals that these bubbles are in

fact generated (by the snap-off mechanism) very near the exit; no motion or indication of bubble production within the bead pack is evident. This result proves that observation of foam bubbles emerging out the end of a porous medium does not ensure that there are foam bubbles inside. It is possible that the bubbles are generated only at the exit.

At gas velocities above ~0.2 cm/s, very small bubbles (roughly 0.05-0.5 mm in diameter) are generated near the inlet to the bead pack. Although this movie does not show clearly how they are generated, Figure 3 shows a frame of the bubbles in the exit region. These bubbles, after generation near the inlet, flow through the pack in a chaotic and wave-like fashion, and, with the exception of a few very large bubbles, they appear fairly monodisperse.

In the second movie, which was taken with a polarized light source at higher magnification levels (~20x), much more is learned about foam generation at the pore level. Here, the primary generation mechanisms are identified; the discovered mechanisms are introduced and described below as "leave behind," "snap off," and "lamella division."

Leave Behind

The leave-behind mechanism, which is shown schematically in Figure 4, is the dominant foam generation mechanism below a critical velocity in homogeneous bead packs. As gas invades a previously liquid-saturated region, it percolates through the many interconnected flow channels. Often, two gas fronts approach the same liquid-filled pore space from different directions. When this happens the liquid in the pore space is squeezed into a lamella by the two fronts. If sufficient surfactant is present in the liquid phase, this lamella may be stable; if not, it ruptures. It is important to realize that this mechanism does not require the two gas fronts to converge simultaneously

on the site; they can arrive at different times and squeeze down the lamella as the local capillary pressure increases.

In highly-connected underground porous media, it is conceivable that this mechanism occurs very frequently. The result is the formation of a large number of lamellae blocking gas pathways. In effect, the lamellae reduce the relative permeability to the gas phase by creating dead-end pathways and blocking flow channels. As shown later, we find a moderate increase in resistance to gas flow as a result of this mechanism. Hence, leave behind generates a relatively weak foam.

There are a few important consequences of the leave-behind mechanism on the foam that is formed. First, no separate gas bubbles are formed by this mechanism of "foam" generation, so the gas remains as a continuous phase. The lamellae which are formed provide a potential "source" for flowing lamellae. Another consequence is that once a lamella generated by leave behind ruptures or flows out of the site, a second lamella cannot be generated at the same site by this mechanism unless liquid reinvades the region.

Leave behind can be observed frequently in the movie. One sequence of frames demonstrating this mechanism is shown in Figure 5. The bubble fronts indicated by the arrows in Figure 5a squeeze together to form a lamella in Figure 5b. In addition to the particular lamella accentuated in Figure 5, four other lamellae which were formed in the same manner are also noticeable. Considering that this frame covers an area of less than ten square bead diameters, it is easy to understand how the leave-behind mechanism can noticeably affect the gas-phase resistance.

Snap Off

Figure 6 illustrates snap off occuring after a gas bubble front

penetrates a constriction and jumps out of the downstream side. (This event is known as a Haines jump or a rheon[9]). As the gas bubble expands, the capillary pressure decreases causing a pressure gradient in the liquid phase for flow from the surrounding liquid into the neck of the constriction. The incoming liquid accumulates at the constriction in a collar, and if the capillary pressure drops below a critical value, the liquid eventually snaps off a gas bubble. Many authors have studied the process of capillary snap off of a nonwetting phase in porous media[10-13]. It is widely believed to be a predominant foam generation mechanism[1,5,14].

Unlike the leave-behind mechanism, snap off creates a separate gas bubble, putting some of the gas into discontinuous form. In addition, it can occur repeatedly at one site, so snap off at a single site can affect a relatively large portion of the flow field.

The snap-off mechanism influences the flow properties of the gas phase by increasing the discontinuity of the gas phase and by creating lamellae. The generated gas bubbles can lodge at some point in the porous medium, thereby blocking gas pathways and creating a similar effect to the lamellae generated by the leave-behind mechanism. Alternatively, the generated bubbles may flow. The resistance to gas flowing in bubble or discontinuous form through porous media is much greater than that to gas flowing as a continuous phase[7]; apparent viscosities for foam flow through porous media on the order of 100 mPa•s are not uncommon[6]. Hence, snap off generates a strong foam.

Snap off is observed to be more important at higher injected flow rates. The sequence of movie frames shown in Figure 7 portrays snap off occurring as a gas bubble invades a constriction and expands out the downstream side. A gas-bubble front at the neck of a constriction is indicated in Figure 7a. As the bubble front expands out the downstream side

of the constriciton (the bubble front is indicated again in Figure 7b), liquid flows back into the neck and snaps off a bubble in Figure 7c.

A different manifestation of the snap-off mechanism is shown in Figure 8 where snap off occurs at a constriciton which is not closely connected to a bubble front. Comparison of Figures 8a and 8b shows that liquid is invading the indicated constriction as the local capillary pressure decreases. The other gas-liquid interfaces in the vincinity also appear to be receding. Eventually, the capillary pressure drops below the critical value in the indicated constricition, and snap off occurs in Figure 8c. This form of snap off is caused by events external to the gas thread undergoing breakup, such as a change in local liquid saturation caused by the displacement of liquid upstream of the constriction.

Lamella Division

Lamella division is different from the first two mechanisms in that it requires a moving lamella; in other words, some type of foam generation must have already occurred. It is more properly a shaping or secondary generation mechanism. This mechanism can occur wherever a lamella approaches a branch point in the flow field. At such a location the lamella and the gas in front of it can flow either into two or more channels downstream of the branch point or into only one of the downstream channels. In the latter case, no division occurs; neither the lamella nor the bubble are altered. However, in the former case, which is illustrated schematically in Figure 9, one lamella is divided into two or more lamellae.

A sequence of frames in which this mechanism is observed is presented in Figure 10. The gas bubble indicated in Figure 10a is forced to flow into the branch point indicated in Figure 10b. As the lamella at the rear of the

bubble approaches the branch point, the bubble divides into the two bubbles indicated in Figure 10c.

The features of this mechanism are very similar to those of the snap-off mechanism: a separate gas bubble is formed, which can either flow or block gas pathways, the mechanism can occur numerous times at one site, and it is seen to be more important at higher gas velocities. Therefore, it is difficult to distinguish between the lamella-division and snap-off mechanisms without looking at the pore-level mechanics. Due to this fact, in later sections of the paper, the generation of fine foam, which occurs almost certainly by a combination of the snap-off and lamella-division mechanisms, is referred to simply as generation by snap off.

Comparison to Previous Work

Previously, little work has been devoted towards identifying the mechanisms of foam generation in porous media. The few authors who have studied foam generation in transparent micromodels have arrived at seemingly varied results.

Using an etched glass plate as a micromodel, Mast[14] was apparently the first to attempt to understand the mechanisms of foam generation through visual observation. Mast described the snap-off and lamella-division mechanisms as being the most important in foam generation. Although he noticed the leave-behind mechanism, he viewed it as unimportant and "not efficient."

More recently, Owete and Brigham[15] also performed foam generation experiments in transparent micromodels. However, aided by the recent development of microelectronic technology, they were able to design the micromodels quite precisely. Two different micromodels were employed: a

homogeneous one, on which a regular closely packed design was etched, and a heterogeneous one, on which a more random design was etched. With the heterogeneous micromodel, foam was generated by the snap-off mechanism. However, no snap off of gas bubbles was seen in experiments done on the homogeneous model. Instead, they observed only the leave-behind mechanism. Lamella division was not mentioned.

Because the three foam generation mechanisms of leave behind, snap off, and lamella division have been observed in other types of porous media[14,15], we contend that they are relevant to all types of porous media. However, their relative importance clearly depends on the characteristics of the particular porous medium and on the experimental conditions. We therefore pursue an experimental study on the effects of velocity, fractional flow, bead size, permeability variations, and surfactant structure on the relative importance of the three foam generation mechanisms.

FOAM GENERATION EXPERIMENTS

Two types of experiments, "quantitative" and "qualitative", are described in this section. In the quantitative experiments, the effects of permeability, flow rate, and fractional flow on the gas-phase relative permeability are determined from measured pressure-drop data. The qualitative experiments are concerned with qualitative and semi-quantitative observations on the effects of permeability variations and surfactant type on the foam generation process.

Quantitative Studies

Gas and, in some cases, gas and liquid are injected at constant,

predetermined flow rates into an initially liquid-saturated bead pack. As noted previously, the experiment is run until either the gas forms a continuous flow path through the bead pack or a fine foam is generated due to the onset of snap off inside the bead pack. In the former case, the gas-phase pressure drop is recorded or estimated after a prolonged steady state is achieved. This measurement represents the viscous contribution to the gas-phase pressure drop at the given flow rate. When the pressure drop rises dramatically due to the massive generation of tiny foam bubbles, the experiment is stopped to prevent damage to the transducer. This result is recorded as a "snap-off" point. No specific steady-state pressure measurement can be taken for the snap-off points with the low-pressure transducers being used, but the fact that snap off is the dominant generation mechanism under the given conditions is a datum in and of itself.

In Figure 11, data are presented in the form of a reduced pressure drop versus a capillary number for a wide range of flow rates and bead sizes. The reduced pressure drop is, by definition, $\Delta p_{nw}K/\mu_{nw}U_{nw}L = 1/k_{nw}$, where Δp_{nw} is the gas-phase pressure drop (inlet - exit), μ_{nw} is the gas-phase viscosity, U_{nw} is the superficial velocity of the gas phase, L is the length of the bead pack, and k_{nw} is the relative permeability to the gas phase. The capillary number is the ratio of gas-phase viscous forces to tension forces, $Ca = \mu_{nw}ULR_g/\sigma Kk_{nw}$, where U is the total superficial velocity, R_g is the bead radius, and σ is the surface tension. Note that, for reasons described in the theory section, the scaling of the capillary number in this paper is different from that traditionally used, $Ca = \mu_w U/\sigma$. there is a difference of approximately a factor of 10^5 between the two capillary numbers. Open data points and snap-off points (labelled by arrows) represent experiments with a 1% (w/w) solution of SDBS; filled-in data points represent runs with

deionized, distilled water.

A number of conclusions may be deduced from Figure 11. At low flow rates, Ca < ~ 10, the presence of surfactants moderately reduces the relative permeability to the gas phase in comparison to the experiments with pure water for all bead sizes. This moderate increase in resistance, about a factor of 5, in the presence of surfactants is due to the leave-behind mechanism; a weak foam exists in the pack. However, above a critical capillary number, Ca^* the relative permeability to the gas phase is dramatically reduced. At this point visual observation shows the onset of snap off within the pack and the generation of a fine-textured, strong foam.

Another important and unexpected result, which is seen in Figure 11 for the data both with and without surfactants, is that the relative permeability to the gas phase is different for 0.5 and 1 mm beads. This could be due to channeling, wall effects, gravity effects, an increase in leave behind and gas-path tortuosity for the lower bead sizes, or a lower displacement by the gas in tighter packs.

Finally, it is interesting to note that in the deionized water experiments. the reduced pressure drop declines beyond a capillary number of about 1. This indicates that more pores are being entered and opened for flow by the displacing gas phase. Therefore, the saturation of the liquid in the pack decreases, and the capillary pressure increases. When surfactants are present, the eventual result of this capillary pressure rise is in-situ snap off.

The effect of fractional flow is also studied. Results are presented in Figure 12 for the case of 1 mm beads. It is evident that the general features of the previous figure are retained. However, Ca^* increases slightly with the fractional flow of liquid.

These experiments illustrate that a critical capillary number exists for strong foam generation in homogeneous bead packs. Strong foam is due to the onset of snap off and lamella division as the dominant foam generation mechanisms. Below the critical capillary number, a weak foam exists in the porous medium due to the leave-behind mechanism.

Qualitative Studies

Effect of Permeability Variations. Underground, oil-bearing porous media are heterogeneous with regions of tight sands opening into loose sands and vice versa. Several simple experiments were performed to investigate the role of macroscopic permeability variations. In these experiments, a portion of the bead pack is filled with 0.5 mm beads while the remainder is packed with 1 mm beads. This creates a situation in which either a region of low permeability opens into a region of high permeability, or a region of high permeability leads into a region of low permeability. Snap off is observed at all velocities at the low-high permeability change boundary, (i.e., as the gas flows from a low to a high permeability region). However, no snap off is observed below Ca^* at the high-low permeability change boundary. This idea will be amplified in the theory section.

Perhaps even more interesting than the results on snap off at a permeability-increase boundary are the observations on what occurs to the gas bubbles after they have been generated. At low velocities, a newly formed bubble percolates through the stagnant, previously formed bubbles and deposits itself at the end of the bubble region (or in the exit region). In this situation, the fraction of moving gas is very low compared to the fraction of stagnant gas. Above a critical velocity, the previously stagnant bubbles start to flow. Once flowing, these bubbles are then further shaped by lamella

division thus creating a much finer foam with both a higher resistance to flow and a higher fraction of moving gas. This is similar to the critical-velocity phenomenon observed in the homogeneous bead packs. It is a plausible explanation for the non-Newtonian behavior of foam flow observed in porous media[6].

Effect of Surfactant Type. The emphasis in this part of the work lies in determining how surfactant structure affects the mechanisms of foam generation. The surfactants used in this study are, as outlined in the experimental section, SDBS, SDS, Chaser SD1000, and Suntech IV 1035. SDS is a straight chain alkyl sulfate. Chaser belongs to the alkyl sulfonate class of surfactants; it is difunctional and highly branched. Suntech IV belongs to the alkyl aryl sulfonate class as does SDBS.

SDBS and SDS exhibit essentially identical behavior over the range of parameters studied. The onset of snap off occurs at similar values of Ca^* and the degree of leave-behind is similar. The industrial surfactants behave differently. Chaser shows similar behavior to SDBS and SDS in 1 mm bead packs, but in tighter bead packs the onset of snap off occurs at higher capillary numbers (or not at all) over the range of flow rates studied. Suntech IV displays similar behavior to Chaser (onset of snap off at higher velocities) in all size bead packs. In addition, the industrial surfactants exhibit stronger flow resistance than either SDBS or SDS at low capillary numbers, suggesting that they form a denser, more persistent leave-behind foam.

Surface tensions of the surfactants, shown in Table 2, do not provide an explanation for the differences in observed behavior. Kanda and Schechter[16] argue that surface viscosities may be important. Without further work, we

cannot draw definitive conclusions.

SNAP-OFF THEORY

To explain quantitatively the origin of the critical capillary number for the onset of snap off, we propose a theory based on the idea of "germination sites". The model relies on a static analysis of the snap off of a perfectly nonwetting phase in a homogeneous bead pack comprised only of regions of regular close-packed spheres. However, incorporation of the dynamics of the snap-off process and of the irregular geometries characteristic of real porous media into the model are briefly discussed. Our main goal is to provide a physical and quantitative understanding of the factors influencing the relative importance of snap off to foam generation.

Static Criterion for Snap Off

Roof's[10] analysis of the snap off of oil droplets in toroidal constrictions provides the static criterion for the snap off of a nonwetting phase in a pore constriction. The criterion is geometric and is presented briefly here for the cases of a circular and a noncircular constriction with a perfectly wetting phase residing next to the solid surfaces.

In a circular constriction, the following inequality must hold for liquid to flow from the front of a bubble in a pore body into the constriction neck and commence snap off:

$$R_b > \frac{2R_c R_g}{R_g - R_c}, \qquad (1)$$

where R_b is the radius of the pore body, R_c is the radius of the constriction, and R_g is the grain or bead radius. In a constricted pore which is sufficiently noncircular in cross section, the static criterion for snap off is slightly different:

$$R_b > \frac{\tilde{C}_m R_c R_g}{R_g - R_c}, \qquad (2)$$

where $\tilde{C}_m = C_m R$ is the dimensionless interfacial curvature, and R is the radius of the largest inscribed circle in the noncircular pore. $\tilde{C}_m$ depends only on the geometry of the pore cross section. For example, if the walls of the pore are three equal-sized beads with their centers arranged so that they form an equilateral triangle, $\tilde{C}_m$ is equal to 1.75. Mayer and Stowe[17] and Ransohoff, Gauglitz, and Radke[18] present more detailed analyses of the configurations of gas-liquid interfaces in noncircular pores, along with tabulated values of $\tilde{C}_m$.

Because the static snap-off criteria are strictly geometric, snap-off behavior of a given porous medium, neglecting dynamic effects, is a function only of the geometric characteristics of the porous medium. To evaluate R_b, R_g, and R_c, the next section presents a brief discussion on the possible pore throat and pore body sizes in homogeneous bead packs.

Pore Throat and Body Sizes in Homogeneous Bead Packs

The pore-throat and pore-body distributions for bead packs may be predicted using the regular close-packing arrangements that can be achieved with monodisperse solid spheres. As shown in Figure 13, there are three types of pore bodies arising from three-dimensional regular close-packing

arrangements. Hexagonal close packing (hcp) and face center cubic packing (fcc) exhibit triangular constrictions with tetrahedral and octahedral pore bodies. Cubic close packing (ccp) has square constrictions and cubic pore bodies. Sizes of all of the constrictions and bodies are given in Table 3 in terms of the radius of the largest inscribed sphere in each constriction or body normalized by the grain radius. The thesis of Ransohoff contains a detailed description of the calculations[8]. In the last two columns of Table 3 the ratios of the body and constriction radii are compared with the snap-off criterion given in Equation (2).

One- and two-dimensional close-packing arrangements are also considered to account for the packing of the beads near the walls and corners of the flow cell. The two-dimensional arrangements are hcp and square packing; the associated constrictions and bodies are shown in Figure 14. Constrictions for both two-dimensional packings are formed by two beads touching below a flat plate. The pore-body characteristic of two-dimensional hcp is that of three beads arranged in a triangle on a flat plate. Likewise, square packing has a characteristic pore body of four spheres arranged in a square on a flat plate. One-dimensional regular packing is simply a straight row of beads along a corner; the constriction and body of which are depicted in Figure 14. As with the three-dimensional packing arrangements, the ratio of body radius to constriction radius for the different one- and two-dimensional packing arrangements is compared to the Roof criterion for the different sites in Table 3.

An interesting result which arises from these geometric calculations is that, in a one-layer homogeneous bead pack which exhibits only one- and two-dimensional close-packing arrangements, the Roof criterion for snap off cannot be met. It is evident that the only geometry that meets the static

requirement for snap off is the octahedral pore body. In the terms of this simple picture, pore throats opening into octahedral pore bodies are the only locations in which snap off can occur. We designate such locations as "germination sites." Of course, gas must enter the sites for snap off to be the dominant foam generation mechanism in a homogeneous bead pack. These arguments lead to the conclusion that the capillary pressure must be high enough to enter the constrictions with a normalized radius, R_c/R_g, of approximately 0.16 for snap off to be the dominant foam generation mechanism in homogeneous bead packs.

Germination Sites in Porous Media

Unlike idealized homogeneous bead packs, naturally occurring porous media contain pore throats and bodies of many different sizes. Therefore, a more general method than that presented in the previous section must be developed to establish the possible germination sites in porous media from the pore-throat and pore-body distributions.

Pore-size distributions can be determined by a number of methods. Mercury porosimetry is the most commonly used technique; it was first proposed by Washburn[19] in 1921. Numerous improvements on the technique and interpretation of the data have been made since then[17,20,21]. However, mercury porosimetry only gives information about the throat-size distribution. Recently, other techniques such as sectional micrography[22] have been used to develop a more precise understanding of the morphology of porous media.

In general, any porous medium can be represented by a series of interconnected pore bodies and pore throats[23] each having its own size distribution. These can be approximated by a set of general distributions

such as that proposed by Mohanty and Salter[24]:

$$g(x_i) = \frac{x_i}{x_{i2}^2} \exp(-x_i^2/2x_{i2}^2) \quad \text{for } x_i \leq 1 \ , \tag{3}$$

$$g(x_i) = 0 \quad \text{for } x_i > 1 \ ,$$

where

$$x_i = \frac{R_i - R_{i,min}}{R_{i,max} - R_{i,min}} \ ,$$

$$x_{i2} = \frac{\overline{R_i} - R_{i,min}}{R_{i,max} - R_{i,min}} \ ,$$

and i is either c (for the pore-throat distributions) or b (for the pore-body distributions). $R_{c,min}$ is the minimum throat radius , $\overline{R}_c$ is the average throat radius, and $R_{c,max}$ is the maximum throat radius. The distributions given in Equation (3) require six input parameters ($R_{i,min}$, $\overline{R}_i$, $R_{i,max}$; i=c,b); these distributions are shown in Figure 15 for a physically reasonable set of parameters.

The static criterion for snap off can be applied to these distributions to obtain a probability that a given pore throat will be connected to a large enough pore body to constitute a germination site. For example, assuming equilateral triangular cross sections, a nonwetting phase in a constriction of

radius $R_c = 0.3\ R_g$ must be connected to the same phase in a pore body of radius $R_b > 0.75\ R_g$, according to the static criterion given in Equation (2), for snap off to occur by liquid flowback from the bubble front into the constriction.

With the pore-size distribution functions $g(x_c)$ and $g(x_b)$ known, the snap-off criterion can be extended to predict the probability that a particular size pore throat will allow snap off. The probability of snap off in a throat of radius R_c is given by the probability that the pore body into which that constriction opens is larger than aR_c, where a is specified as follows:

$$a = \frac{\tilde{C}_m R_g}{R_g - R_c} \quad . \tag{4}$$

$\tilde{C}_m$ is the dimensionless interfacial curvature as discussed previously. Using $g(x_b)$, we calculate the probability, G, that a pore body radius will be greater than aR_c as follows,

$$G(R_c/R_g) = 1 - \frac{\int_0^{x^*} g(x_b)dx_b}{\int_0^1 g(x_b)dx_b} , \tag{5}$$

where $x^* = (aR_c - R_{b,min})/(R_{b,max} - R_{b,min})$. Equation (5) can be integrated to provide a more convenient expression of this probability:

$$G(R_c/R_g) = 1 - \frac{\exp(-x^{*2}/2x_{b2}^2) - 1}{\exp(-1/2x_{b2}^2) - 1} \quad \text{for } x^* > 0 , \qquad (6)$$

$$G(R_c/R_g) = 1 \quad \text{for } x^* < 0 .$$

If the joint probability distribution for the connection of pore throats and pore bodies is not weighted at all, then G is also the probability of snap off in a constriction of radius R_c. In other words, G specifies the probability that a given pore-throat size is connected to a large enough pore body to be a germination site. Assuming that the flow channel cross sections are equilateral triangles, and that the joint probability distribution is unweighted, the snap-off probability distribution is calculated for the pore-size distributions given in Equation (3) and plotted in Figure 16. As can be seen in Figure 16, there is no probability of snap off in the larger pore constrictions. They are never connected to large enough pore bodies to meet the Roof criterion. Conversely, there is a very high probability of snap off in the smaller throats. Thus, germination sites tend to be the smaller pore throats.

Another useful way of looking at the germination-site concept is from the perspective of the standard capillary pressure-saturation curve given in Figure 17[25]. This figure shows that, along both the imbibition and drainage curves, the magnitude of the the slope, dP_c/dS_w increases as the wetting-phase saturation decreases. Therefore, as the smaller pores (low S_w) are entered by the nonwetting phase, small increases in liquid saturation can produce a large decrease in capillary pressure, resulting in snap off in the small pores. However, a much larger increase in liquid saturation is required to produce

the same drop in capillary pressure in the larger pores, making snap off in these pores less likely. This view applies not only to the "Roof" type of snap off which is due to expansion of a gas bubble out of a constriction but to snap off due to any event which causes a local increase in liquid saturation. Thus, it is apparent that, regardless of the cause of the local capillary pressure drop, snap off is much more likely in smaller constrictions than in larger ones, reinforcing the contention that the germination sites are the smaller pore throats.

Activation of Germination Sites

Although the smaller pore throats are more likely to be the location of the snap-off sites, it is extremely unlikely that the smallest pore throats will be invaded by the nonwetting phase due to the high capillary pressure required for entrance. Therefore, it is in the medium-sized constrictions that snap off will occur.

It is this idea which leads to the concept of activating the germination sites. There are three requirements for a germination site to be active. The first is that the capillary pressure be high enough so that the nonwetting phase is able to enter or impregnate the site:

$$p_{nw} - p_w > -\frac{\tilde{C}_m \sigma}{R_c} \quad . \tag{7}$$

The second requirement arises from the dynamics of liquid flow back into the constriction. Specifically, the capillary pressure must be below the critical value for long enough to allow the wetting liquid to flow back into the constriction and initiate snap off. The third requirement is that there

be enough liquid available locally to allow for snap off. The first two requirements are discussed later in some detail.

Using the germination-site concept, the results of the permeability-increase experiments described in the qualitative studies section can be easily explained. In these experiments, snap off was observed at all velocities at the permeability-increase boundary between low and high permeability regions. It is evident that, at this boundary, there are many small constrictions in the low permeability regions which are connected to large bodies in the high permeability region. Therefore, nearly every flow channel leads to a germination site at the boundary, and snap off is expected at all velocities. This is the same phenomenon as the "exit" foam observed in the visual experiments and depicted in Figure 2. In the exit region, the permeability change is from a finite permeability region to one of essentially infinite permeability. Indeed, exit foams are always expected, clouding the issue of foam generation within a non-transparent porous medium.

Entrance of Germination Sites

Our next step is to describe the flow conditions under which the germination sites are entered by the nonwetting phase. In the experiments underlying Figure 11, gas is injected into a homogeneous bead pack saturated with an aqueous surfactant solution. Below the critical capillary number, the gas fingers through the pack until a steady state is achieved in which no liquid is produced. Visual observations indicate that the liquid saturation in this situation is considerably above the connate or irreducible liquid saturation. The balance of viscous and capillary forces pertinent to this problem is quantified by the fractional flow equation of Leverett[26]:

$$f_w \equiv \frac{U_w}{U} = \frac{1 + \frac{Kk_{rnw}}{U\mu_{nw}}\left(\frac{dP_c}{dz}\right)}{1 + \frac{\mu_w k_{nw}}{\mu_{nw} k_{rw}}} \tag{8}$$

In the experiments described above, the wetting-phase fractional flow, f_w, is equal to zero at steady state, and we simplify Equation (8) to

$$\frac{U\mu_{nw}}{Kk_{rnw}} = -\left(\frac{dP_c}{dz}\right). \tag{9}$$

There is no wetting liquid flow over a given length because the nonwetting-phase pressure drop is equal to the capillary pressure decline, leaving the wetting-phase pressure constant. Equation (9) integrates to give

$$\frac{\mu_{nw} U L_r}{Kk_{rnw}} = P_{c1} - P_{c2} \quad , \tag{10}$$

where L_r is the length over which the capillary pressure gradient occurs. Capillary pressures at the upstream and downstream boundaries, P_{c1} and P_{c2}, can be expressed in terms of average radii of curvature, $\bar{r}_1$ and $\bar{r}_2$.

$$P_{ci} = \frac{2\sigma}{\bar{r}_i} \quad . \tag{11}$$

Combination of Equations (10) and (11) gives the following result:

$$Ca \equiv \frac{\mu_{nw} U L_r R_g}{\sigma K k_{rnw}} = 2\left[\frac{1}{\bar{r}_1/R_g} - \frac{1}{\bar{r}_2/R_g}\right] . \qquad (12)$$

Equation (12) justifies the form of the capillary number chosen to represent the flow data in Figure 11. It states that, with $f_w = 0$, higher velocities lead to larger capillary pressure differences over the distance L_r (i.e., a smaller $\bar{r}_1$ relative to $\bar{r}_2$). When U increases to the point where the octahedral germination sites can be invaded by the nonwetting gas phase, then snap off commences. This condition corresponds to the critical capillary number, Ca^*, for strong foam generation seen in Figure 11.

To evaluate Ca^* from Equation (12), a number of parameters must be specified. These include the permeability of the bead pack, K, which is found in Table 1, the relative permeability to gas, k_{rnw}, which is determined from the results shown in Figure 11, and the length of the region, L_r, which is taken to be the length of the bead pack, L, for these experiments. In addition, the curvature terms, $\bar{r}_1$ and $\bar{r}_2$ are evaluated by using the results from the homogeneous sphere packing geometries. The radius of curvature at the exit is assumed to be approximately equal to the radius of the large cubic-packing constrictions, which is found in Table 3 to be $\bar{r}_2 \sim 0.4\ R_g$. (The choice of $\bar{r}_2$ is not crucial. Varying $\bar{r}_2$ from $0.25\ R_g$ to $1.0\ R_g$ changes the resulting critical capillary number by less than a factor of 2). The radius of curvature at the bead-pack inlet is then determined by the viscous pressure drop in the nonwetting phase. According to Table 3, the gas must enter constrictions of radius $\bar{r}_1 = 0.16\ R_g$ to invade the octahedral germination sites in the homogeneous bead pack.

Using these values, the critical capillary number for the onset of snap off can be calculated:

$$Ca^* = 8 \tag{13}$$

Note that the effects of bead size (permeability), flow velocity, and length of communicating liquid are all contained in the critical capillary number, Ca^*, given in Equation (13). In Figure 18, the theory is compared to the experimental data presented earlier in Figure 11. We see that, when the wetting-phase fractional flow in the bead packs is zero, the germination-site model is in excellent agreement with the measured onset of snap off. Also, as noted in the visual experiments, snap off commences towards the front of the bead pack, consonant with the physical picture underlying Equation (13).

At low wetting-phase fractional flows, one would not expect the behavior of the system to change drastically from the case where $f_w = 0$; a capillary pressure gradient should still exist despite the presence of a small wetting-phase pressure drop. Obviously, Equation (9) does not hold in this case; rather, it becomes an inequality:

$$-\left(\frac{dP_c}{dz}\right) < \frac{U\mu_{nw}}{Kk_{rnw}} \tag{14}$$

It is evident from Equation (8) that there is still a balance between U and dP_c/dz which maintains a constant fractional flow. It is this balance which eventually leads to snap off at higher velocities. Therefore, for the case of low to medium wetting-phase fractional flows, the theory for snap off proposed in the previous section should apply semi-quantitatively. Based on the inequality shown in Equation (14), the critical capillary number, Ca^*, should

be slightly greater than the critical capillary number for the zero fractional flow case of Equation (13). The data shown in Figure 12 support this assertion.

Liquid Flow Back in the Germination Sites

There is an additional criterion for the activation of a germination site that arises from the dynamics of the liquid flow into the constriction. Specifically, the capillary-pressure driving force for flow into the constriction must exist for a time interval, t_b, which is longer than the time required for the liquid flow, t_{so}, causing snap off.

To evaluate t_{so}, we utilize the results of Ransohoff, Gauglitz, and Radke[18] who solve an evolution equation for the time to snap off in a constricted noncircular capillary. For specified pore-constriction geometries and fluid properties, these authors calculate the dimensionless time to snap off, $\tilde{t}_{so} = t_{so}/\tau_{so}$, where τ_{so} is equal to $\mu_w R_T/\sigma$ and R_T is the radius of the largest inscribed circle in the unconstricted capillary.

The other half of the flow-back problem is to determine the time over which the capillary pressure will be below the critical value, P_c^*, required for snap off. The case where the capillary pressure drops below P_c^* due to external events is difficult to quantify; however, when the static criterion for snap off is met due to the expansion of a gas bubble out of the downstream side of a constriction, the problem is tractable.

As a gas bubble front moves from a pore throat into a pore body that meets all the other snap-off criteria, it reaches a point where the critical drain-back curvature is met. But as it continues through the pore body, the bubble front eventually moves into another throat, and the local capillary pressure rises above P_c^* again. The time interval, t_b, over which the

capillary pressure is below the ceiling required for snap off can be determined from the following equation,

$$t_b = \int_0^{L_b} \frac{dz}{u_{nw}(z)} \quad , \tag{15}$$

where L_b is the length of the pore body over which the curvature is below the critical value, and $u_{nw}(z)$ is the local bubble front velocity. If $u_{nw}(z)$ is assumed to be the average interstitial gas velocity of the process, which is equal to $U_{nw}/(S_{nw}\phi)$, then Equation (15) can be rewritten as follows:

$$t_b = \frac{\phi S_{nw} L_b}{U_{nw}} \tag{16}$$

If the time to snap off, t_{so}, is less than t_b, gas-bubble break up occurs. If not, the germination site, which would otherwise be active, is not so because the "flow-back" criterion for snap off is not satisfied. In the surfactant-type experiments presented in the qualitative studies section, it was observed that some surfactants show much less tendency to snap off than others. The flow-back criterion for snap off provides a possible explanation for the observed dependence of the snap-off behavior on surfactant type. Specifically, the explanation is that, due to differences in surface rheological properties, the time to snap off and local interstitial velocity of a gas bubble may depend on the surfactant structure. It is possible that, for some surfactant solutions, the time to snap off is greater than the time required for the bubble front to move through the pore body while, for other solutions, it is less. This might explain why some surfactants display a greater tendency to undergo snap off than others. However, independent experiments in constricted square pores[27] reveal very little difference in

the time to snap off for solutions of Chaser SD1000 and SDBS, whereas a significant difference in the snap-off behavior of these two surfactants is observed in bead packs.

CONCLUSIONS

In this paper, the primary mechanisms of foam generation in bead packs are identified and classified as leave behind, snap off, and lamella division. These mechanisms are thought to be general to all types of porous media.

The effect of bead size, velocity, fractional flow, permeability variations, and surfactant type on the relative importance of the foam generation meachanisms in homogeneous bead packs is also determined. The most significant result is that there exists a critical capillary number in homogeneous bead packs above which snap off and lamella division become the dominant generation mechanisms, causing a strong foam to be formed. Below this critical velocity, the generated foam is weaker and is due to the leave-behind mechanism. Increasing the fractional flow of the liquid increases this critical capillary number slightly. In addition, we find that snap off occurs at all velocities when gas flows from a low permeability region into a high permeability region. Finally, the surfactant structure strongly influences the relative importance of the foam generation mechanisms.

The concept of "germination sites", which meet the static, geometric criterion for snap off, is the crucial aspect of our proposed theory for strong-foam generation in porous media. Three criteria must be met for a germination site to be active: the site must be entered by the gas, a dynamic flow-back criterion for snap off must be met, and there must be sufficient

liquid present for snap off to occur. Therefore, the number of active germination sites, and hence the relative importance of the snap-off mechanism, depends on the pore geometry, fluid properties, and capillary and viscous forces. The germination-site model is found to agree quantitatively with the observed snap-off behavior in homogeneous bead packs over a range of bead sizes (0.25 mm to 1.0 mm), gas velocities (0.001 cm/s to 0.3 cm/s), and gas-phase fractional flows (0.6 to 1.0).

The importance of snap off in a porous medium is directly proportional to the number of active germination or snap-off sites. Previously, the number of sites was assumed to be a constant, independent of any process or porous medium parameters[5]. The work presented here shows that this assumption is an unrealistic one, and it provides a basic model that can be used to determine the dependence of the number of active germination sites on various parameters, such as capillary number and porous matrix geometry.

NOMENCLATURE

a = $\tilde{C}_m R_g/(R_g - R_c)$, coefficient used in snap-off criterion

Bo = Bond number, $\Delta\rho g R_g h/\sigma$, ratio of gravity forces to tension forces

Ca = capillary number, $\mu_{nw} U L R_g/\sigma K k_{rnw}$, ratio of viscous forces to tension forces

C_m = interfacial curvature (m^{-1})

$\tilde{C}_m$ = geometric constant, which contains the effect of the noncircular pore cross-sectional shape on the equilibrium curvature

f_w = wetting-phase fractional flow, U_w/U

g = gravitational acceleration constant (9.8 m^2/s)

$g(x_i)$ = probability distribution function for pore throat and pore body

sizes; i = b,c

$G(R_c/R_g)$ = probability that snap off will occur in a constriction of dimensionless radius R_c/R_g

h = height (m)

k_r = relative permeability

K = absolute permeability (m^2)

L_b = length of pore body over which the curvature is below the critical value for snap off (m)

L_r = length of saturation gradient region (m)

P = pressure ($kg/m \cdot s^2$)

P_c = capillary pressure ($kg/m \cdot s^2$)

r_i = radius of curvature at point i (m)

R = radius of largest inscribed circle in a noncircular pore (m)

R_b = pore-body radius (m)

R_c = pore-constriction radius (m)

R_g = grain or bead radius (m)

R_i = average pore throat or body size; i = b,c (m)

$R_{i,min}$ = minimum pore throat or body size; i = b,c (m)

$R_{i,max}$ = maximum pore throat or body size; i = b,c (m)

R_T = radius of the unconstricted pore channel (m)

S_{nw} = nonwetting-phase saturation

S_w = wetting-phase saturation

t_b = time for a gas bubble front to move through a pore body section of length L_b(s)

t_{so} = time to snap off in a constricted noncircular capillary (s)

U = Darcy or superficial velocity (m/s)

u_{nw} = local velocity of the gas bubble front (m/s)

x_i = dimensionless pore throat or body size; i = b,c

x_{i2} = dimensionless average pore throat or body size; i = b,c

z = length scale in the direction of flow (m)

Greek Symbols

μ = viscosity (kg/m•s)

ρ = density (kg/m^3)

σ = surface tension (kg/s^2)

τ_{so} = characteristic time for snap off in a constricted noncircular capillary (s)

ϕ = porosity

Subscripts

w = wetting phase

nw = nonwetting phase

so = snap off

r = region

Superscripts

* = critical

$\bar{}$ = average

$\tilde{}$ = dimensionless

ACKNOWLEDGEMENTS

This work was supported by a Department of Energy Grant DE-AC03-76SF00098 to the Lawrence Berkeley Laboratory of the University of California. T.C. Ransohoff gratefully acknowledges fellowships from the Shell Foundation and the Regents of the University of California.

REFERENCES

1. Fried, A.N.: "The Foam-Drive Process for Increasing the Recovery of Oil," U.S. Dept. of the Interior, Bureau of Mines, Rep. Inv. 5866, Washington, D.C. (1961).

2. Dilgren, R.E., Deemer, A.R. and Owens, K.B.: "The Laboratory Development and Field Testing of Steam/Noncondensible Gas Foams for Mobility Control in Heavy Oil Recovery," paper SPE 10774, presented at the 1982 California Regional Meeting of the SPE, San Francisco, March 24-26.

3. Ploeg, J.F. and Deurksen, J.H.: "Two Successful Steam/Foam Field Tests, Sections 15A and 26C, Midway-Sunset Field," paper SPE 13609, presented at the 1985 California Regional Meeting of the SPE, Bakersfield, March 27-29.

4. Dietz, D.N., Bruining, J. and Heijna, H.B.: "Foamdrive Seldom Meaningful," J. Pet. Tech. (May 1985) 921-922.

5. Falls, A.H., Gauglitz, P.A., Hirasaki, G.J., Miller, D.D., Patzek, T.W. and Ratulowski, J.: "Development of a Mechanistic Foam Simulator: The Population Balance and Generation by Snap-Off," paper SPE 14961, presented at the 1986 SPE/DOE Enhanced Oil Symposium, Tulsa, April 20-23.

6. Treinen, R.J., Brigham, W.E. and Castanier, L.M.: "Apparent Viscosity Measurements of Surfactant Foam in Porous Media," Supri TR-48, Stanford University (1985).

7. Hirasaki, G.J. and Lawson, J.B.: "Mechanisms of Foam Flow in Porous Media: Apparent Viscosity in Smooth Capillaries," Soc. Pet. Eng. J. (April 1985) 176-190.

8. Ransohoff, T.C.: "Foam Generation in Constricted Noncircular Capillaries and Bead Packs," Ph.D. Thesis, University of California (1987).

9. Morrow, N.R.: "Physics and Thermodynamics of Capillary Action in Porous Media," Ind. Eng. Chem. (1970) 62(6), 32-56.

10. Roof, J.G.: "Snap-Off of Oil Droplets in Water-Wet Pores," Soc. Pet. Eng. J. (March 1970) 85-90.

11. Strand, S.R., Hurmence, C.J., Davis, H.T., Scriven, L.E. and Mohanty, K.K.: "Choke-Off of Nonwetting Fluids in Porous Media," unpublished, Univ. of Minnesota, Dept. of Chem. Eng. (1982).

12. Arriola, A., Willhite, G.P. and Green, D.W.: "Trapping of Oil Droplets in a Noncircular Pore Throat and Mobilization upon Contact with a Surfactant," Soc. Pet. Eng. J. (February 1983) 99-114.

13. Gauglitz, P.A.: "Instability of Liquid Films in Constricted Capillaries: A Pore Level Description of Foam Generation in Porous Media," Ph.D. Thesis, Univ. of California, Berkeley (1986).

14. Mast, R.F.: "Microscopic Behavior of Foam in Porous Media," paper SPE 3997, presented at the 1972 SPE Fall Meeting, San Antonio, Oct. 8-11.

15. Owete, O.S. and Brigham, W.E.: "Flow of Foam Through Porous Media," Supri TR-37, Stanford University (1984).

16. Kanda, M. and Schechter, R.S.: "On the Mechanism of Foam Formation in Porous Media," paper SPE 6200, presented at the 1976 SPE Fall Meeting, New Orleans, Oct. 3-6.

17. Mayer, R.P. and Stowe, R.A.: "Mercury Porosimetry - Breakthrough Pressure for Penetration Between Packed Spheres," J. Coll. Int. Sci. (1965) 20, 893-911.

18. Ransohoff, T.C., Gauglitz, P.A. and Radke, C.J.: "Snap Off of a Gas Bubble in a Constricted Noncircular Capillary," in preparation (1986).

19. Washburn, E.W.: "Note on a Method of Determining the Distribution of Pore Sizes in a Porous Material," Proc. Nat. Acad. Sci. (1921) 7, 115-116.

20 Ritter, H.L. and Drake, L.C.: "Pore-Size Distribution in Porous Materials," Ind. Eng. Chem., Anal. Ed. (1945) 17(12), 782-786.

21. Frevel, L.K. and Kressley, L.J.: "Modifications in Mercury Porosimetry," Anal. Chem. (1963) 35(10), 1492-1502.

22. Dullien, F.A.L. and Dhawan, G.K.: "Characterization of Pore Structure by a Combination of Quantitative Photomicrography and Mercury Porosimetry," J. Coll. Int. Sci. (1974) 47, 337-349.

23. Mohanty, K.K.: "Fluids in Porous Media: Two-Phase Distribution and Flow," Ph.D. Thesis, Univ. of Minnesota (1981).

24. Mohanty, K.K. and Salter, S.J.: "Multiphase Flow in Porous Media: II Pore-Level Modeling," paper SPE 11018, presented at the 1982 Annual SPE Meeting, New Orleans, Sept. 26-29.

25. Craig, F.F.: The Reservoir Engineering Aspects of Waterflooding SPE Monograph Series AIME New York (1971).

26. Leverett, M.C.: "Capillary Behavior in Porous Solids," AIME Trans. (1941) 142,152.

27. St. Laurent, C., Gauglitz, P.A. and Radke, C.J.: "An Experimental Study of Snap-Off in Constricted Glass Capillaries of Circular and Square Cross Section," Undergraduate Research Report, University of California, Department of Chemical Engineering and Lawrence Berkeley Laboratory, LBID-1165 (1986).

List of Figures

Figure 9 Schematic diagram of the lamella-division mechanism.

Figure 10 Three movie frames in sequence showing a bubble undergoing division. The gas bubble indicated in (a) approaches the branch point in (b). As the lamella at the rear of the bubble is forced into the branch point, division occurs, and the two bubbles shown in (c) are formed.

Figure 11 Experimental data for the steady-state, gas-phase, viscous pressure drop across an initially liquid-filled bead pack as a function of flow rate. Data are presented in the form of an inverse relative permeability against a capillary number. "Snap-off" points represent capillary numbers at which snap off dominates the foam generation process. They do not represent steady-state pressure measurements. In these experiments, the injected fractional flow of gas is 1.0, the liquid phase is either deionized, distilled water or 1 wt.% SDBS, and the nominal bead size is 0.25 mm, 0.5 mm, or 1.0 mm.

Figure 12 Experimental data for the steady-state, gas-phase, viscous pressure drop across an initially liquid-filled bead pack as a function of flow rate and fractional flow rate of gas. Data are presented in the form of an inverse relative permeability against a capillary number. "Snap-off" points represent capillary numbers at which snap off dominates the foam generation process. They do not represent steady-state pressure measurements. The nominal bead size for these experiments is 1.0 mm, the injected fractional flow of gas is 0.6, 0.8, or 1 0, and the liquid phase is 1 wt.% SDBS.

Figure 13 Three-dimensional regular close packing arrangements of monodisperse spheres.

Figure 14 One- and two-dimensional regular close packing arrangements of monodisperse spheres.

Figure 15 Pore-throat and pore-body distributions calculated from the distributions given in Equation (3) with the following parameters: $R_{c,min}$ = 0.1 R_g $R_{c,max}$ = 0.5 R_g, $\overline{R_c}$ = 0.25 R_g $R_{b,min}$ = 0.35 R_g, $R_{b,max}$ = 0.9 R_g and $\overline{R_b}$ = 0.55 R_g.

Figure 16 Snap off probability as a function of constriction radius as calculated by Equation (6) for the pore-throat and pore-body size distributions given in Figure 15.

Figure 17 Schematic representation of a standard capillary pressure versus saturation diagram (after Craig[25]).

Figure 18 Comparison of experimental data presented in Figure 11 with the theory for the onset of snap off at Ca^* = 8.

Table 1 Absolute permeability and porosity values for 0.25 mm, 0.5 mm, and 1.0 mm bead packs.

Bead Diameter, $2R_g$ (mm)	Absolute Permeability, K (μm^2)	Porosity, ϕ
1.0	370	0.36
0.50	140	0.37
0.25	40	0.34

Table 2 Surface tensions of surfactants used in foam generation experiments. All measurements are taken at 1 wt.%.

Surfactant	Surface Tension (mN/m)
SDS	37
SDBS	31
Chaser SD 1000	40
Suntech IV 1035	32

Table 3 Pore constriction and pore body radii for regular close packing arrangements of monodisperse spheres. Critical R_b/R_c values are calculated assuming that the pore channel has a cross-sectional shape of three adjacent beads ($\tilde{C}_m = 1.75$), except in the case of three-dimensional cubic packing where a cross section of four adjacent beads ($\tilde{C}_m = 1.86$) is used.

Packing Arrangement	R_c/R_g	R_b/R_g	R_b/R_c	Critical R_b/R_c
One-dimensional	0.172	0.354	2.06	2.11
Two-dimensional HCP	0.250	0.333	1.33	2.33
Two-dimensional Square packing	0.250	0.500	2.00	2.33
Three-dimensional Tetrahedral body	0.155	0.228	1.47	2.07
Three-dimensional Octahedral body	0.155	0.414	2.67	2.07
Three-dimensional Cubic body	0.414	0.732	1.77	3.17

Foam Generation Apparatus

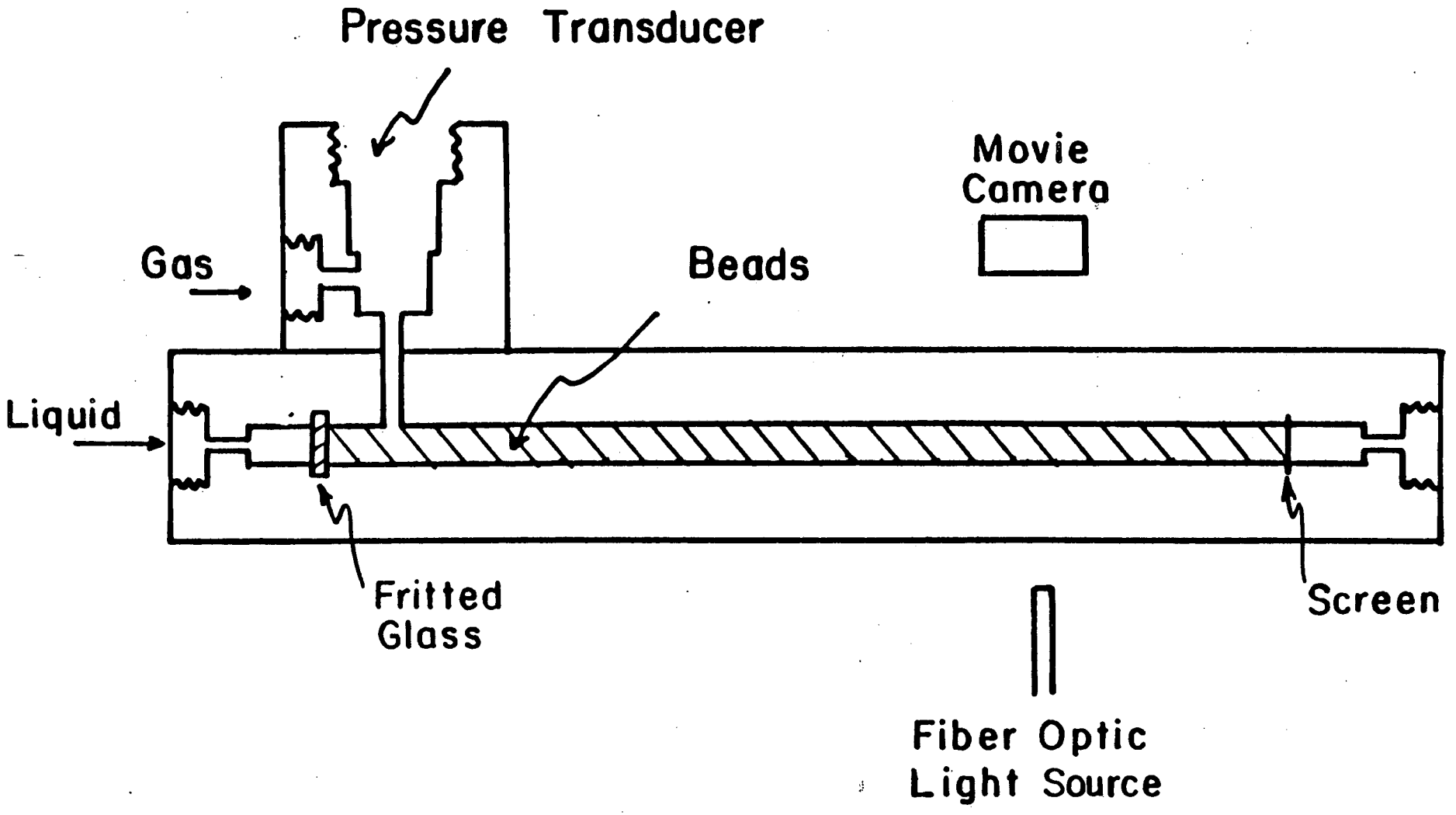

Figure 1

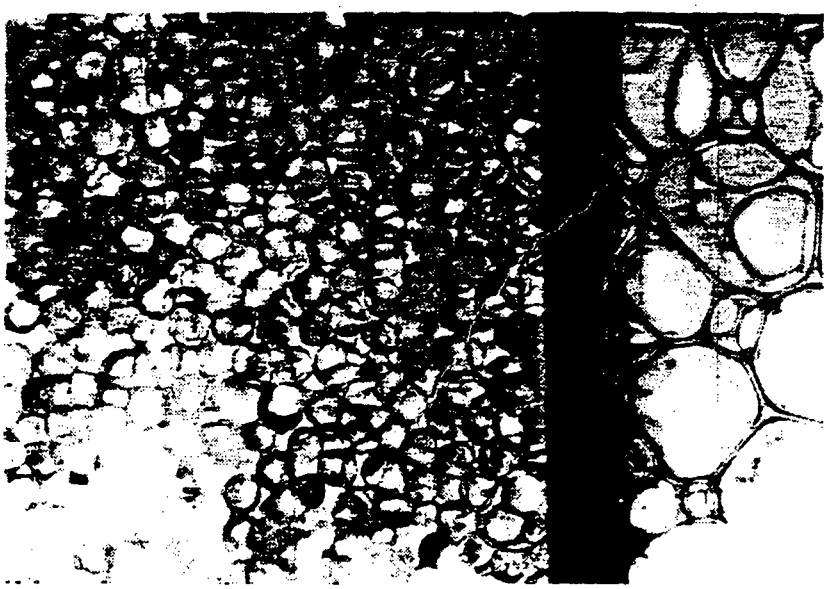

Figure 2 Large gas bubbles characteristic of the "exit" foam generated at low gas velocities. The exit of the bead pack lies to the right of the dark vertical line.

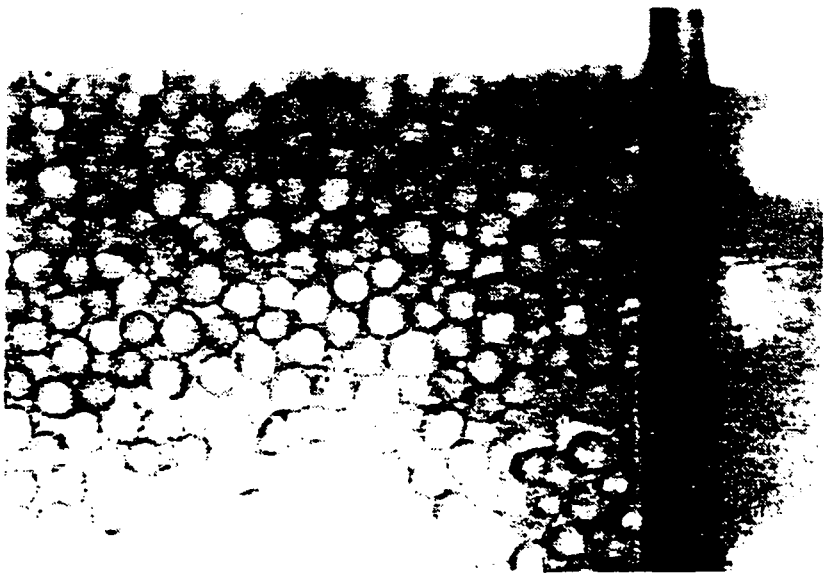

Figure 3 Fine bubbles (characteristic of a strong foam) generated in the bead pack at high gas velocities. The exit of the pack lies to the right of the dark vertical line.

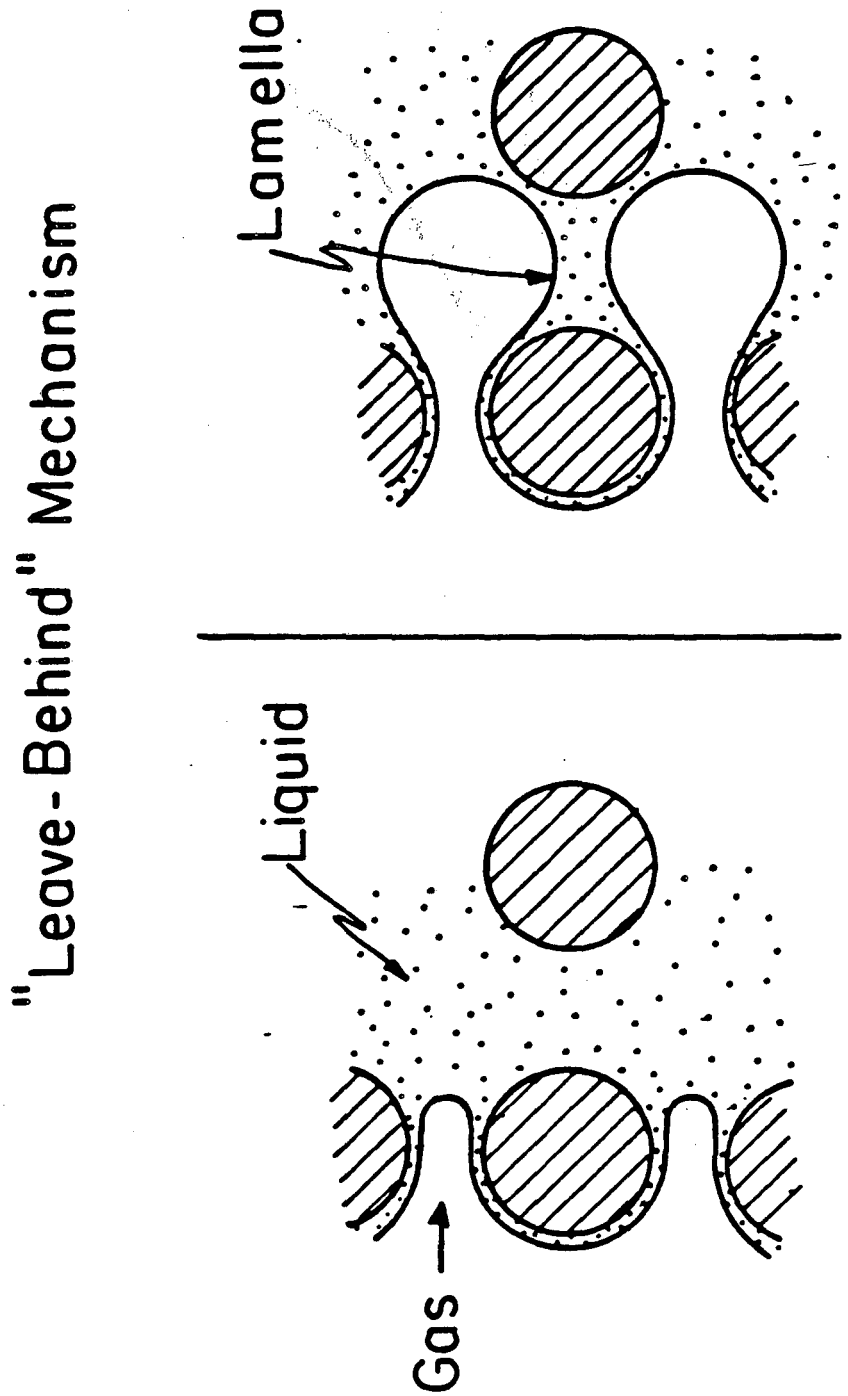

Figure 4

(a)

(b)

Figure 5 Two movie frames in sequence showing the leave-behind mechanism. The arrows in (a) show two bubble fronts that will squeeze together to form a lamella in (b).

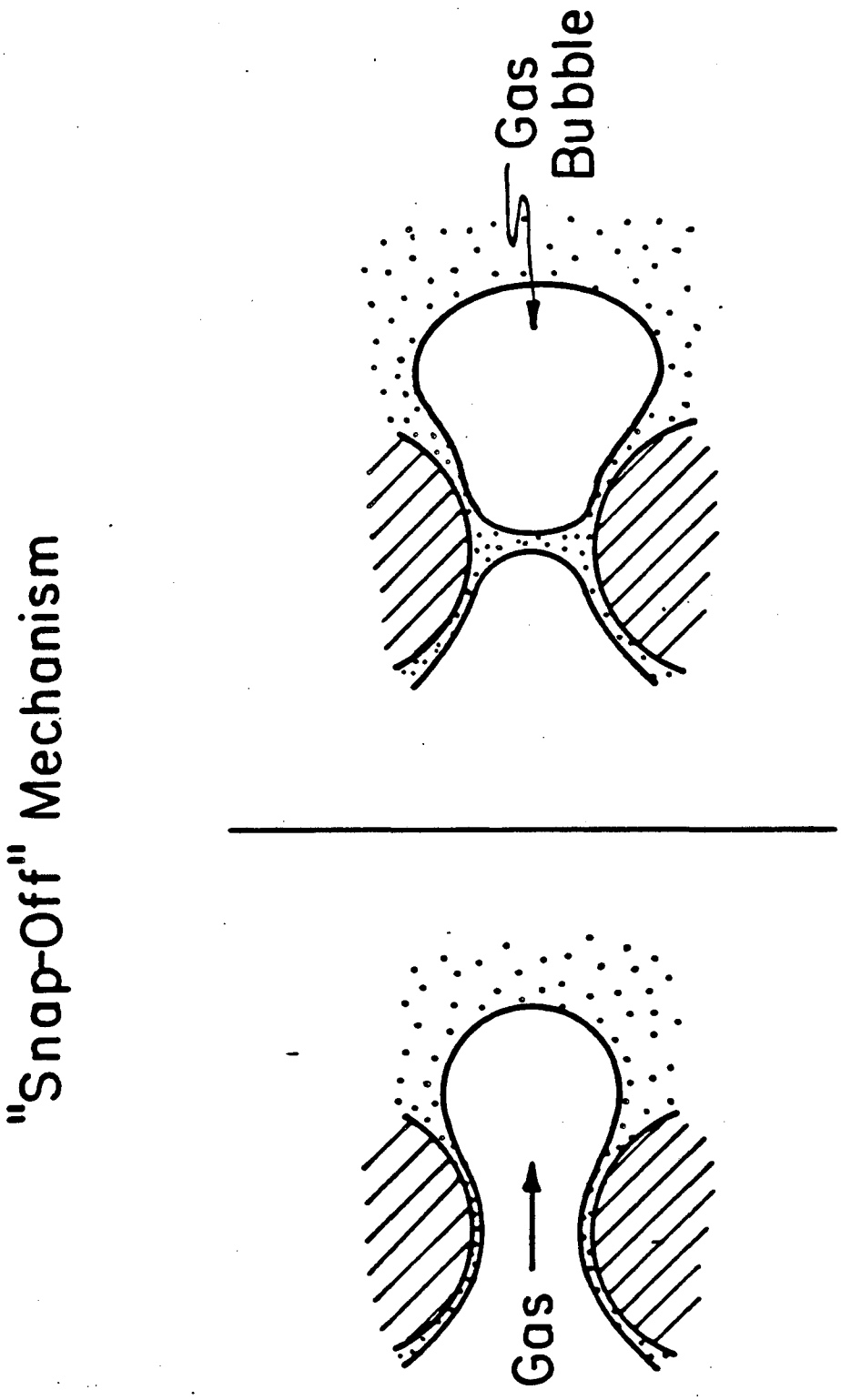

Figure 6

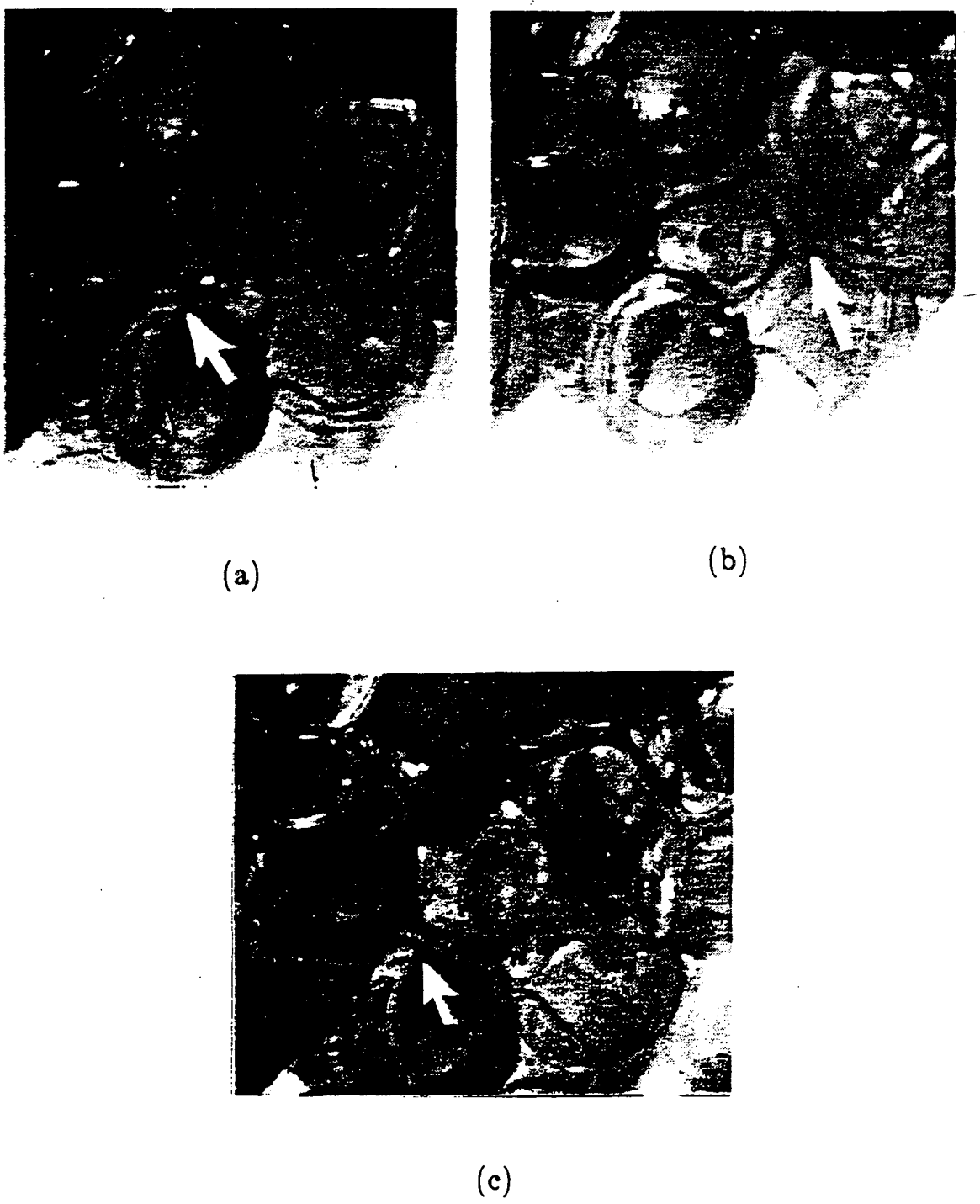

Figure 7 Three movie frames in sequence, which depict the snap-off mechanism occurring due to the expansion of a gas bubble out of a constriction. Arrows in (a) and (b) indicate the front of a gas bubble, first at the neck of the constriction, and subsequently expanding into the adjacent pore body. The result of this expansion is seen to be the formation of a liquid lamella at the neck of the constriction, as shown in (c).

(a)

(b)

(c)

Figure 8 Three movie frames in sequence illustrating the occurence of snap off due to a local drop in capillary pressure. The arrows in (a) and (b) indicate a constriction that has previously been invaded by gas. In (b) liquid reinvades the region, and in (c), the local liquid saturation has increased to the point where snap off occurs at the indicated constriction.

"Lamella-Division" Mechanism

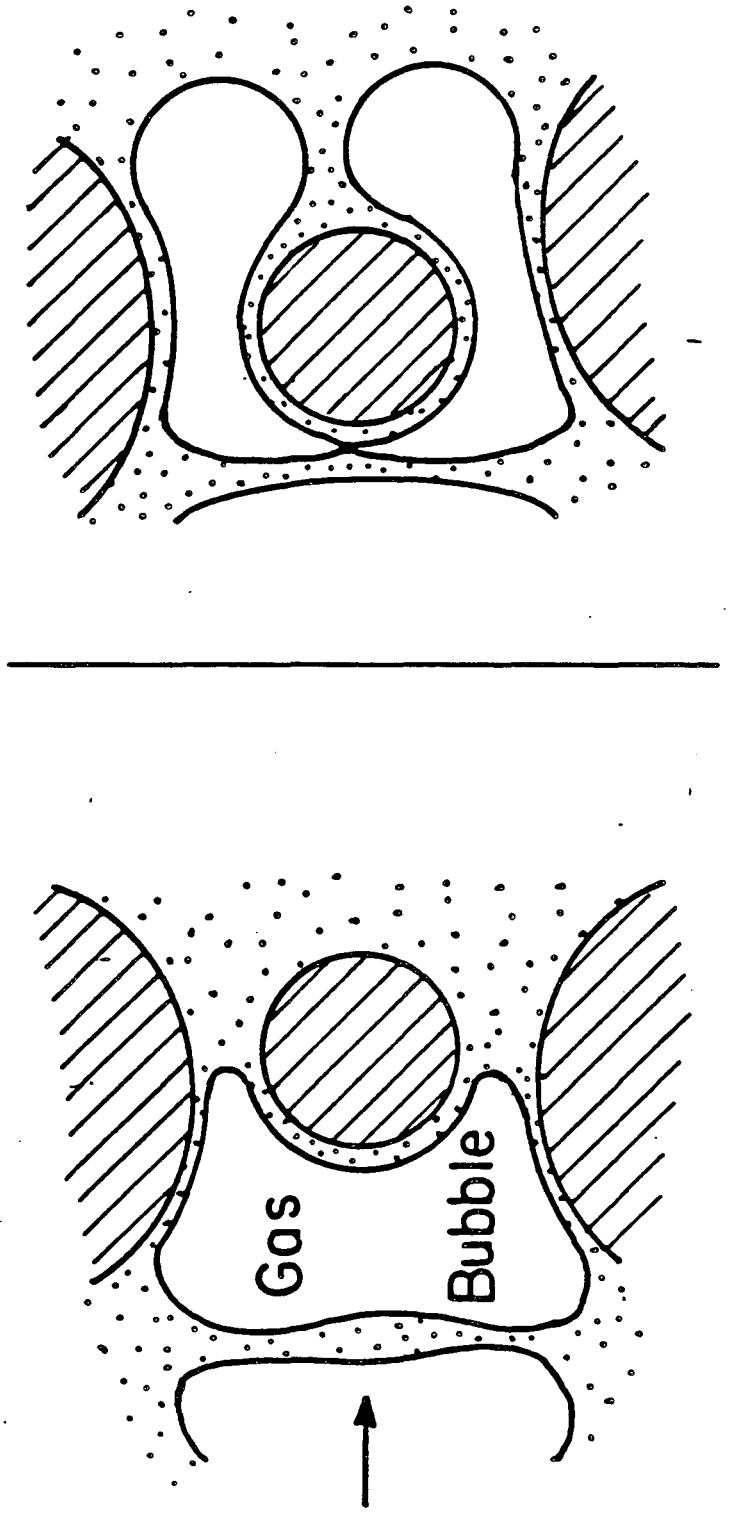

Figure 9

Figure 10 Three movie frames in sequence showing a bubble undergoing division. The gas bubble indicated in (a) is seen to approach the branch point in (b). As the lamella at the rear of the bubble is forced into the branch point, division occurs, and the two bubbles shown in (c) are formed.

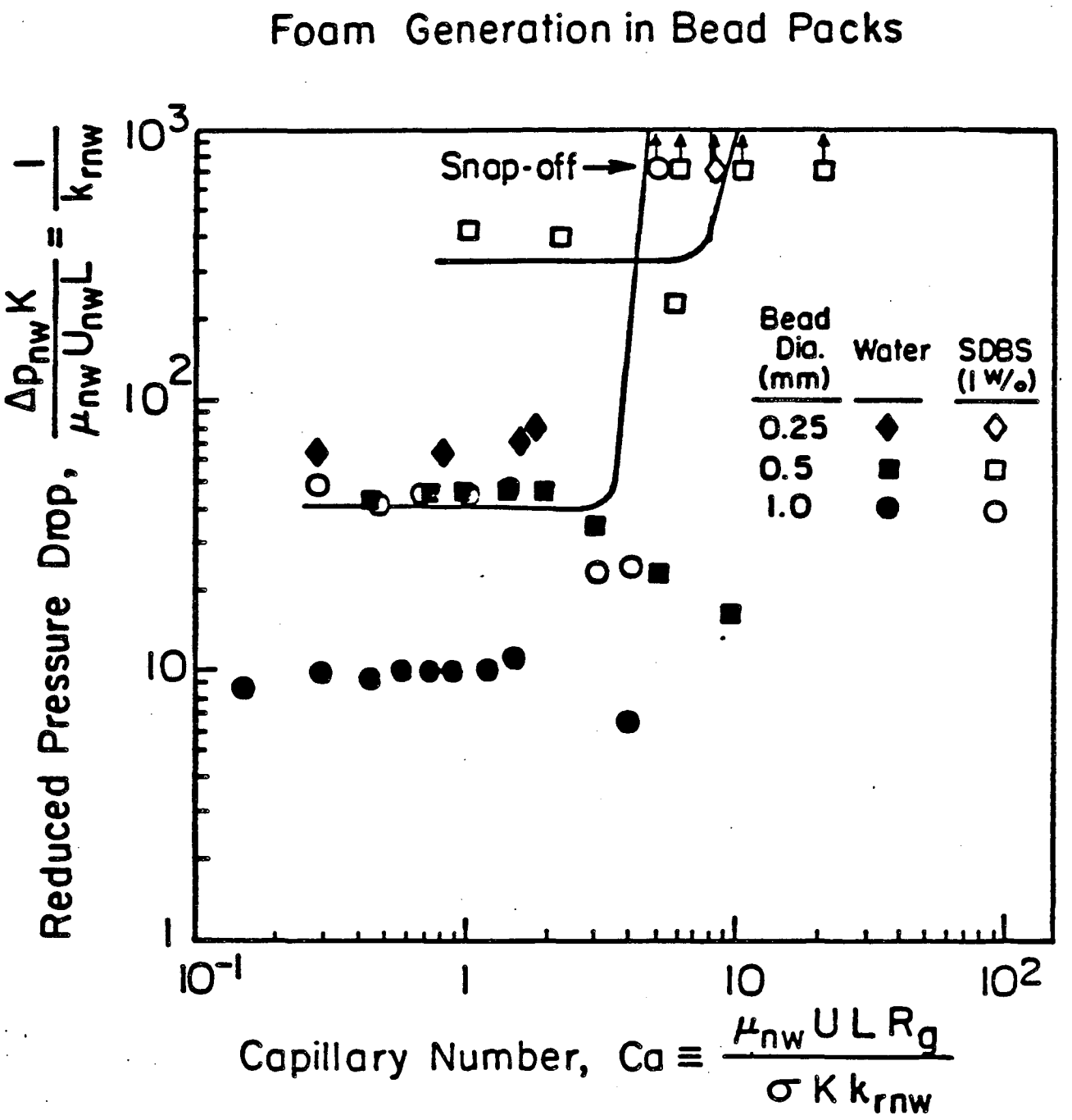
Foam Generation in Bead Packs
Snap-off
Bead Dia. (mm)
Water
SDBS (1 W/o)
0.25
0.5
1.0
Reduced Pressure Drop, $\frac{\Delta p_{nw} K}{\mu_{nw} U_{nw} L} = \frac{1}{k_{rnw}}$
10^3
10^2
10
1
10^{-1}
1
10
10^2
Capillary Number, $Ca \equiv \frac{\mu_{nw} U L R_g}{\sigma K k_{rnw}}$

Figure 11

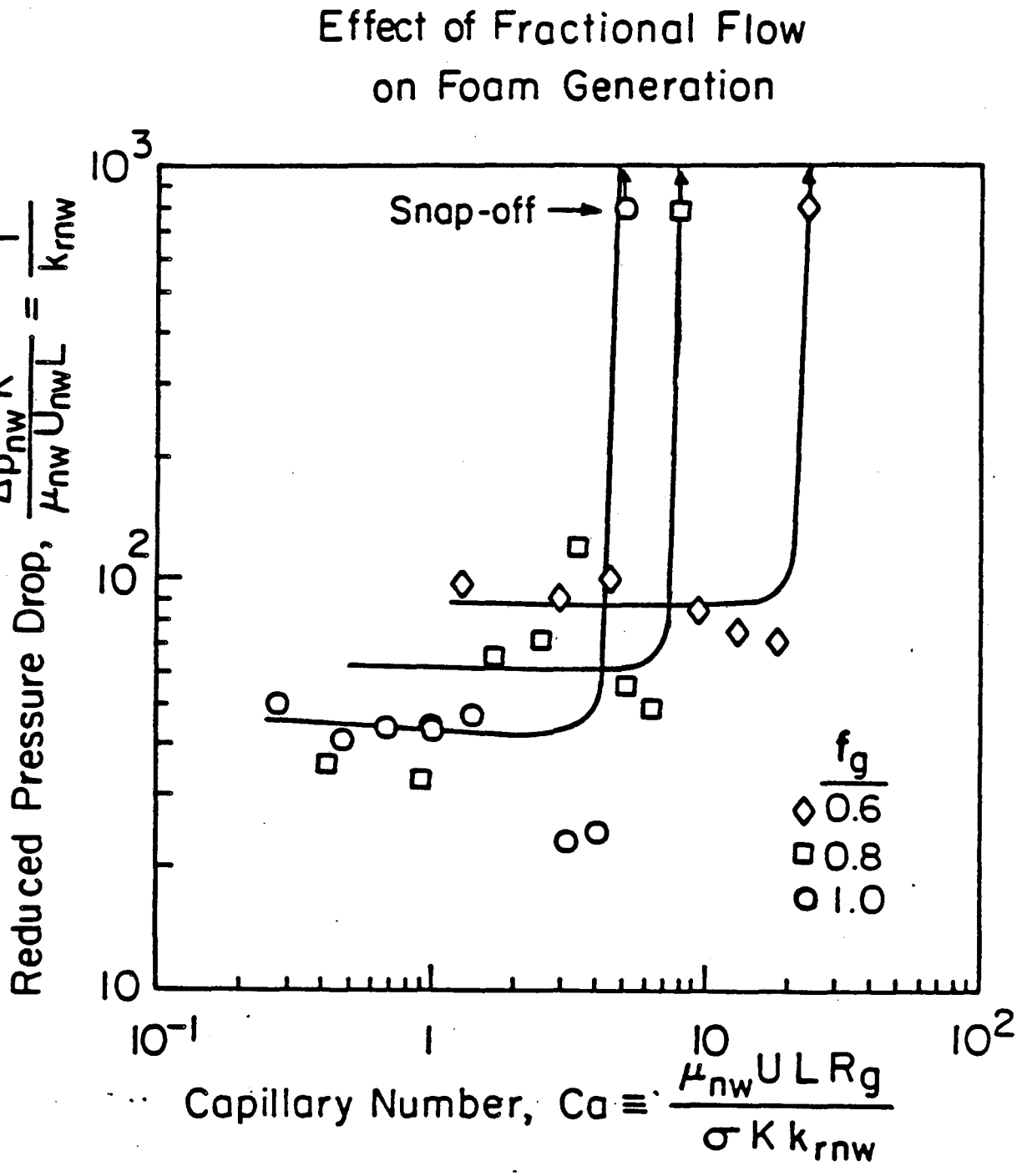
Effect of Fractional Flow
on Foam Generation
Snap-off
f_g
0.6
0.8
1.0
10^3
10^2
10
10^{-1}
1
10
10^2
Reduced Pressure Drop, $\frac{\Delta p_{nw} K}{\mu_{nw} U_{nw} L} = \frac{1}{k_{rnw}}$
Capillary Number, $Ca \equiv \frac{\mu_{nw} U L R_g}{\sigma K k_{rnw}}$

Figure 12

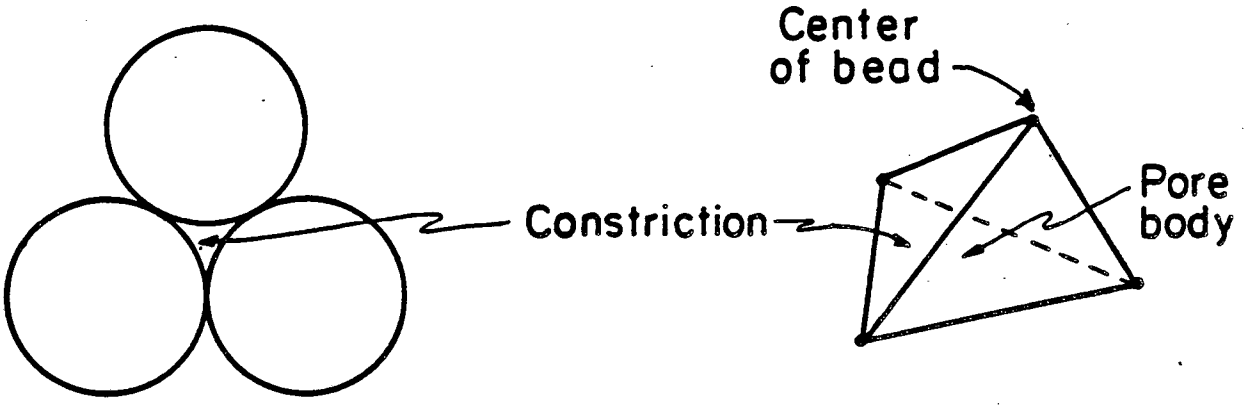

TETRAHEDRAL PORE BODY

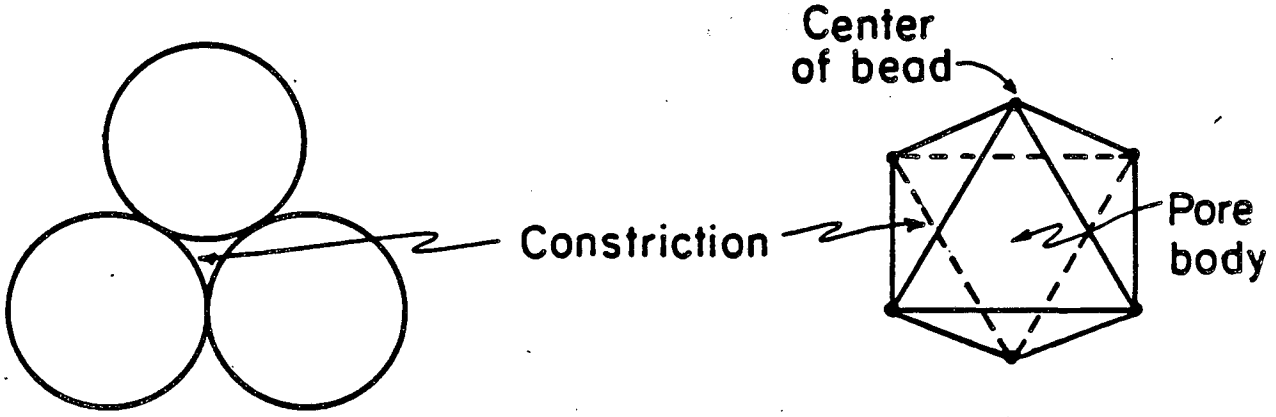

OCTAHEDRAL PORE BODY

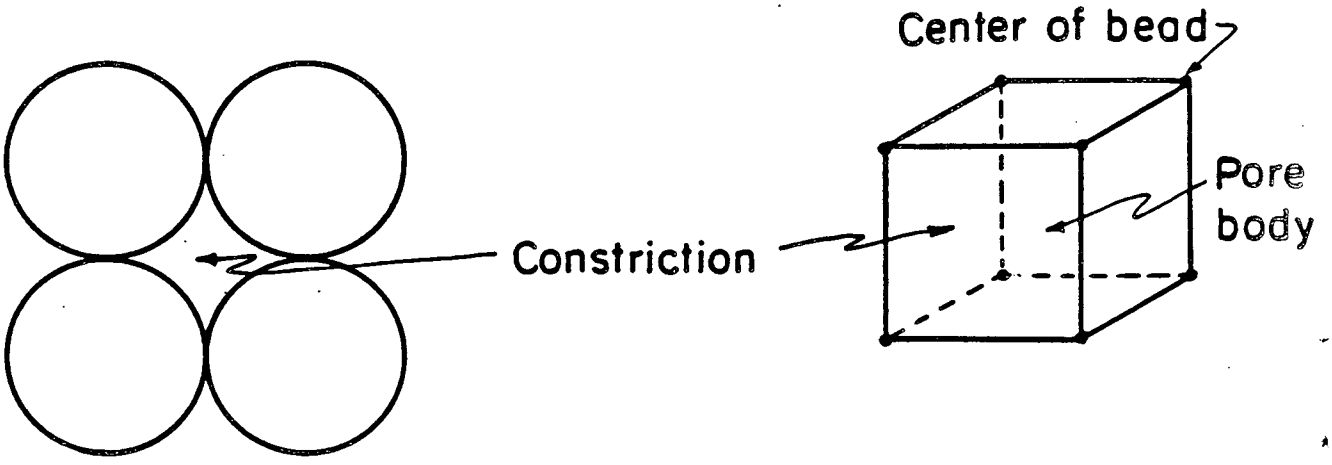

CUBIC PORE BODY

Figure 13

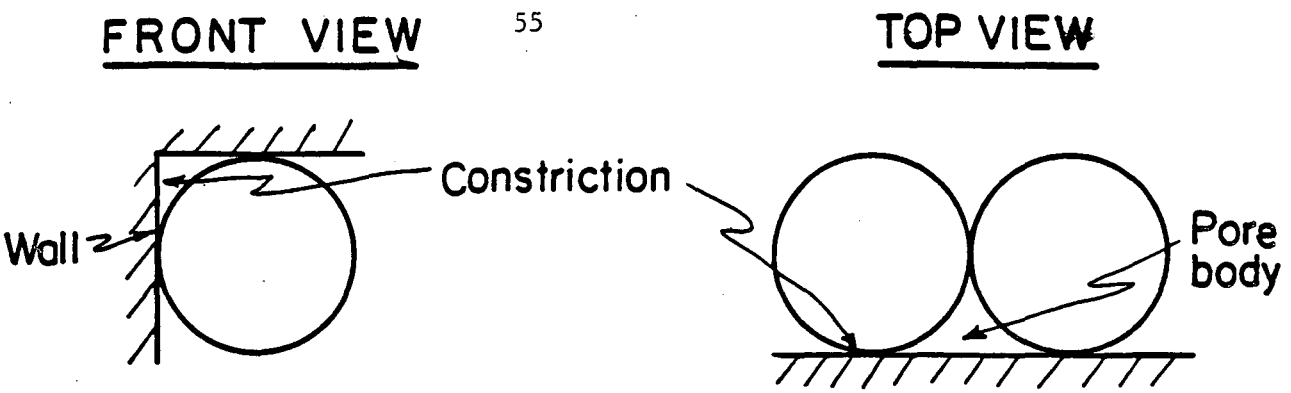

ONE-DIMENSIONAL ARRANGEMENT

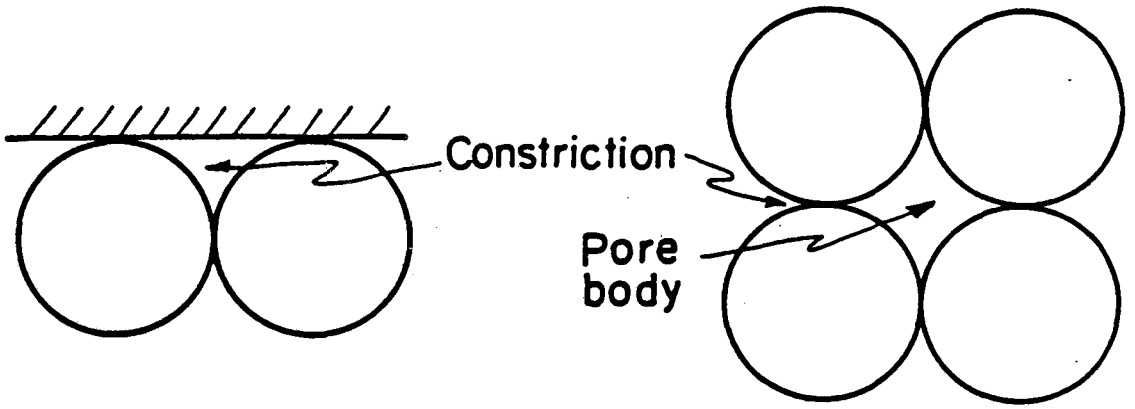

TWO-DIMENSIONAL SQUARE PACKING

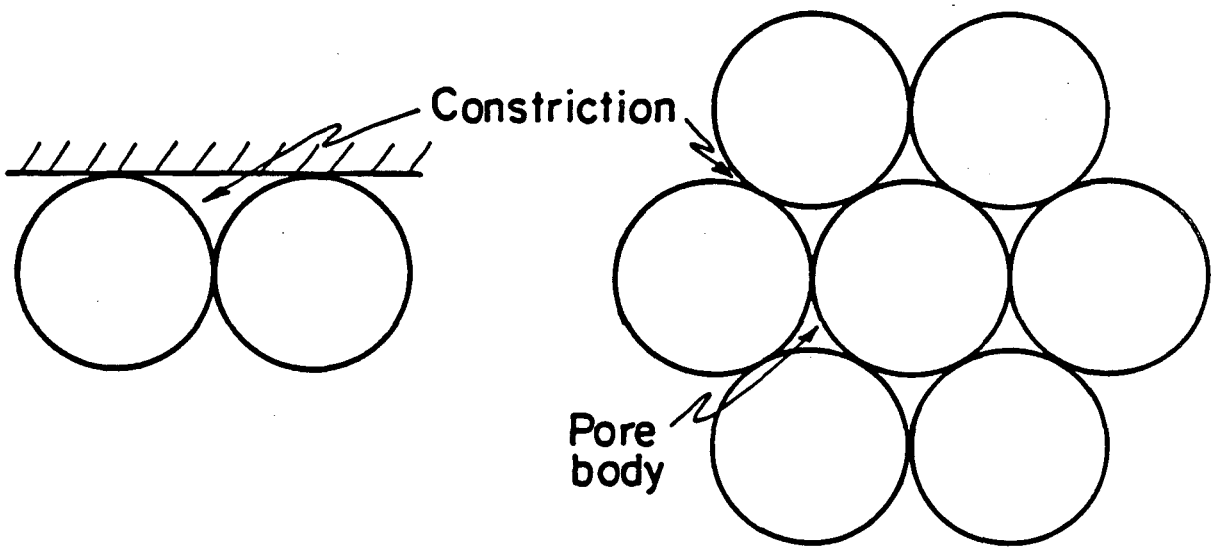

TWO-DIMENSIONAL HEXAGONAL CLOSE PACKING

Figure 14

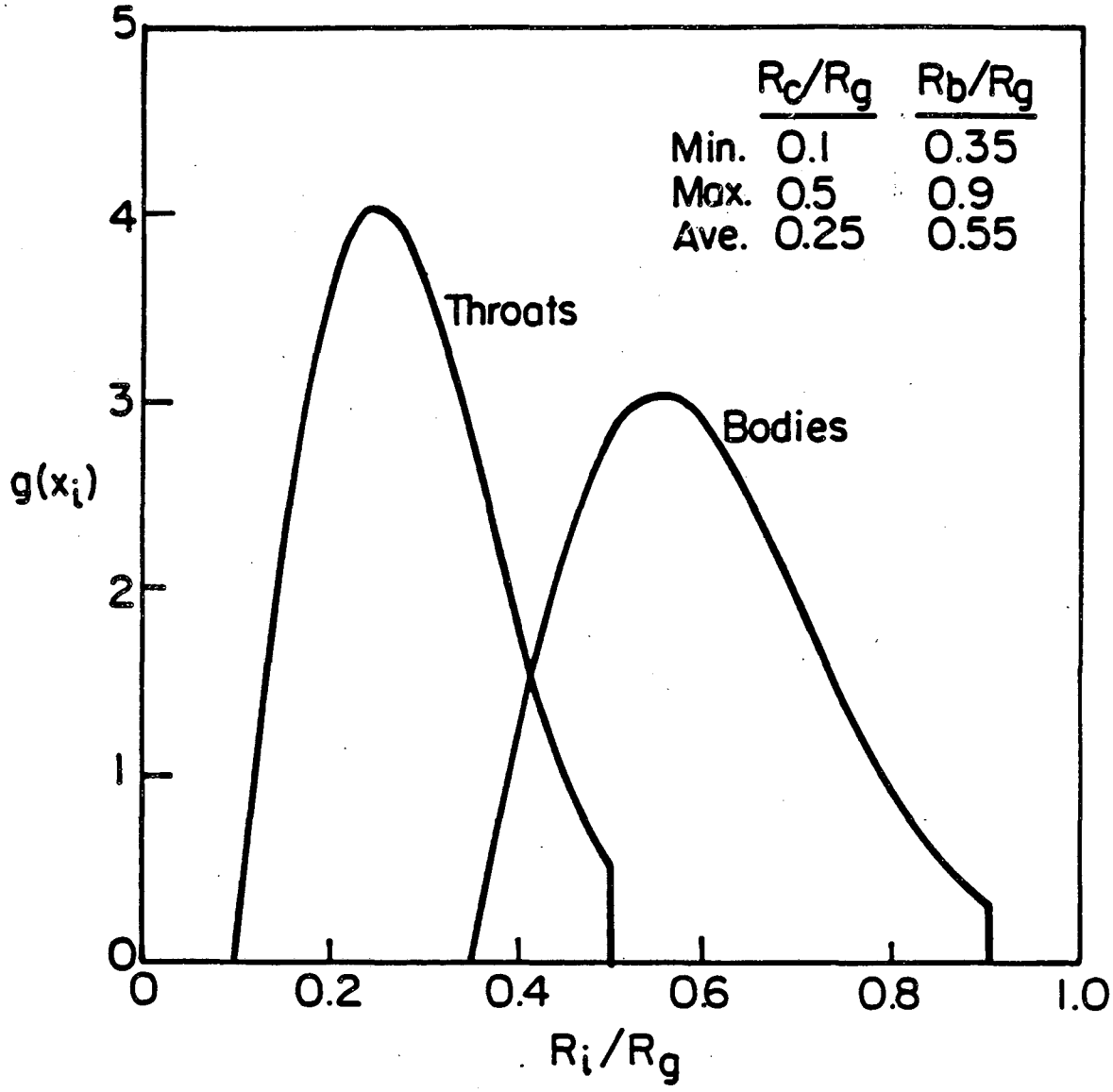
5
4
3
2
1
0
g(x_i)
0
0.2
0.4
0.6
0.8
1.0
R_i/R_g
R_c/R_g
R_b/R_g
Min. 0.1 0.35
Max. 0.5 0.9
Ave. 0.25 0.55
Throats
Bodies

Figure 15

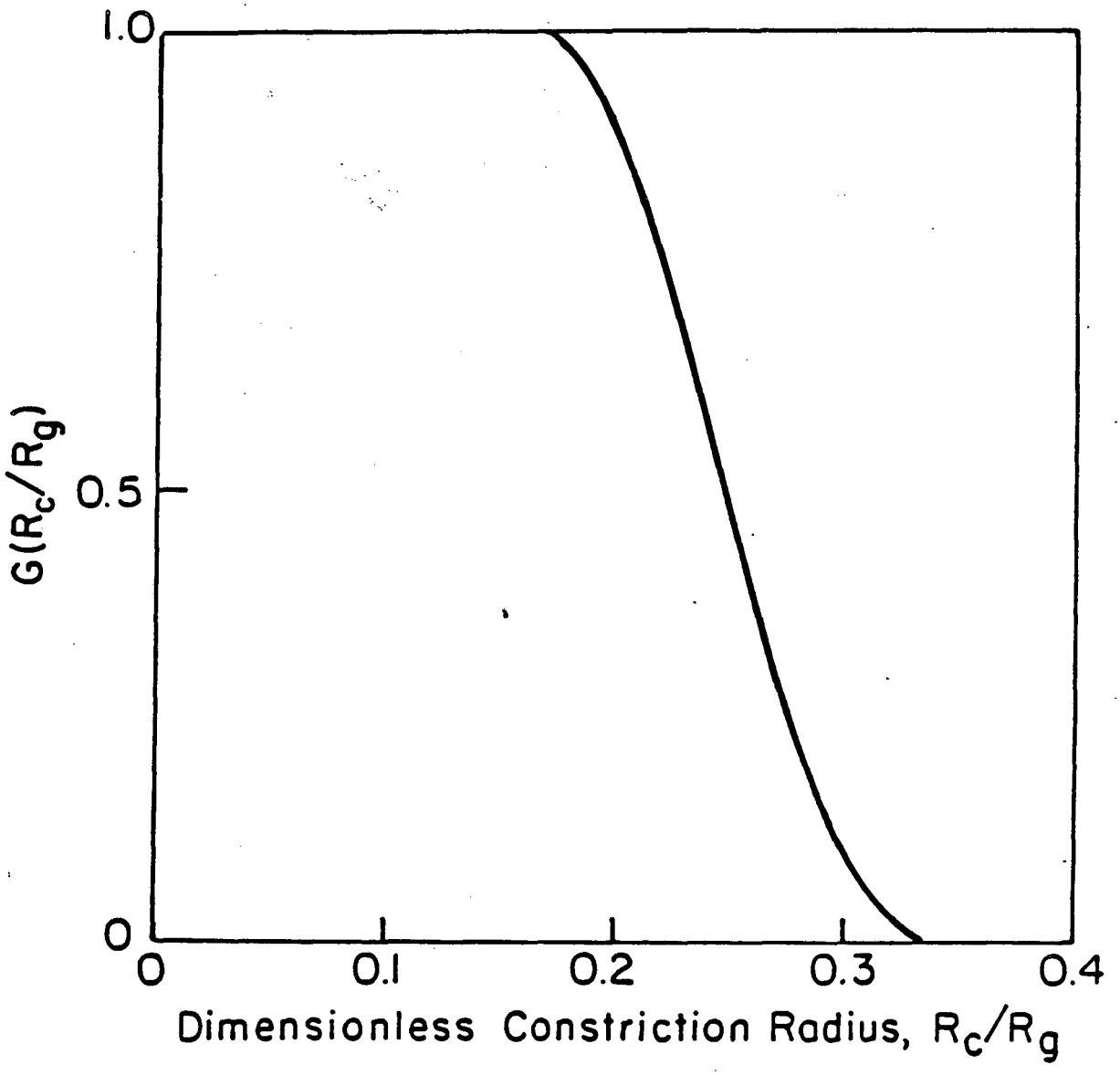
1.0
0.5
0
$G(R_c/R_g)$
0
0.1
0.2
0.3
0.4
Dimensionless Constriction Radius, R_c/R_g

Figure 16

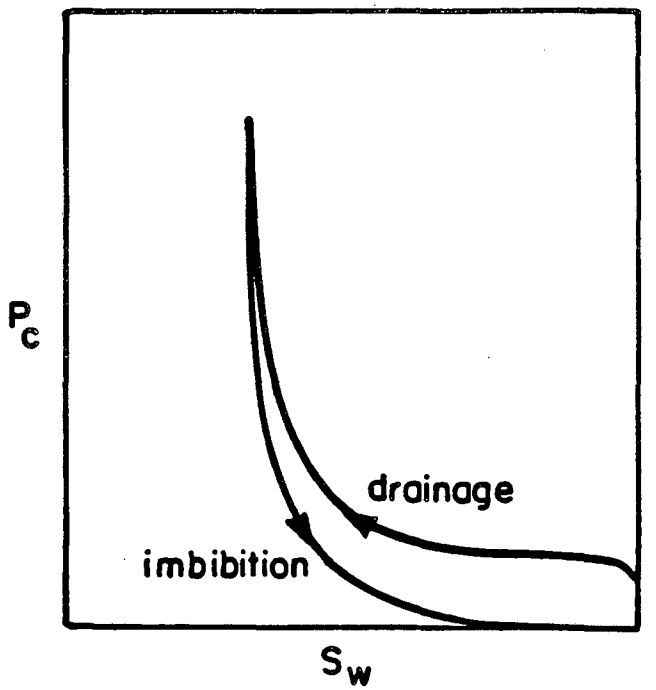

Figure 17

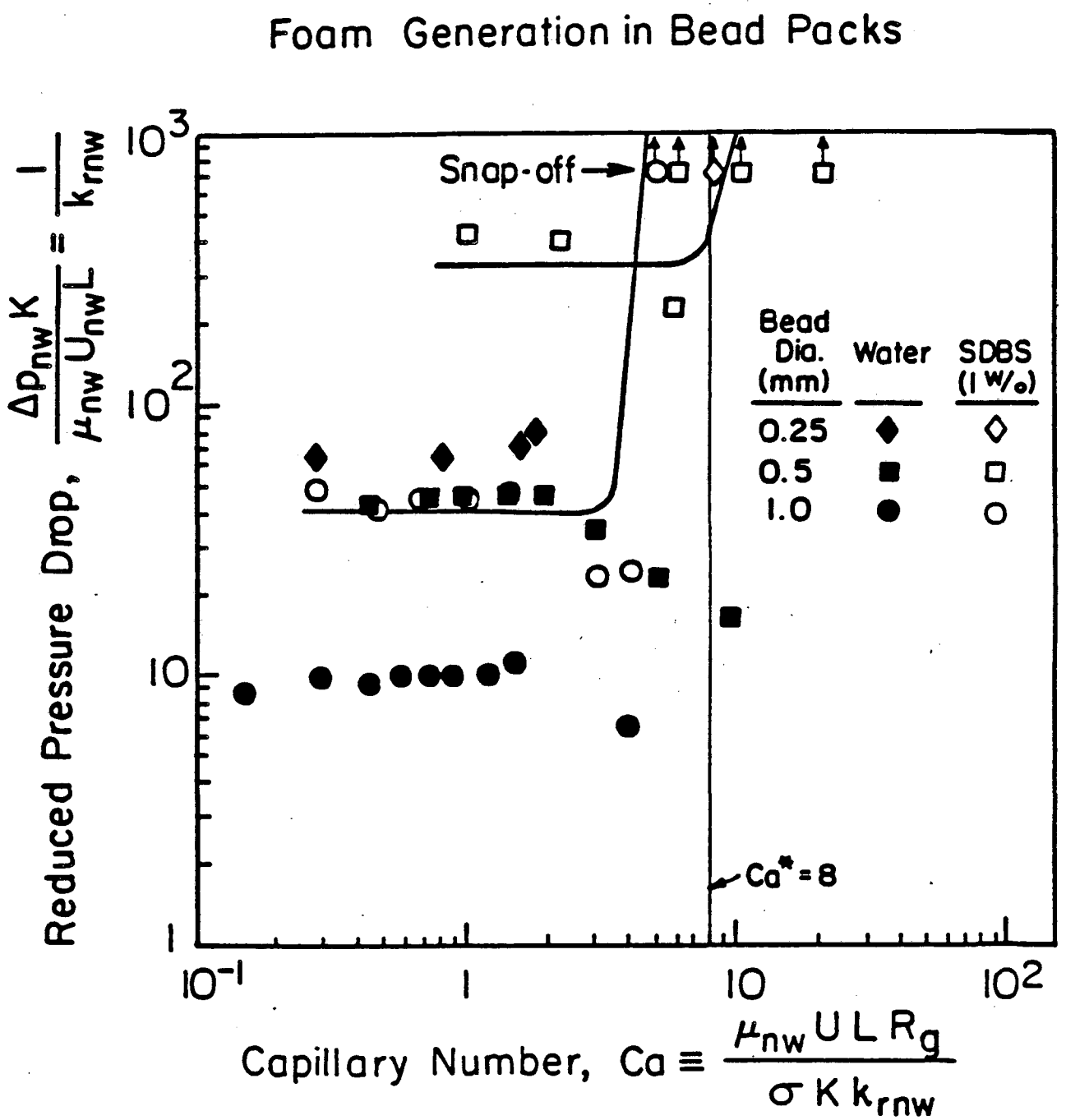
Foam Generation in Bead Packs
Reduced Pressure Drop, $\frac{\Delta p_{nw} K}{\mu_{nw} U_{nw} L} \equiv \frac{1}{k_{rnw}}$
10^3
10^2
10
1
Snap-off
Bead Dia. (mm)
Water
SDBS (1 W/o)
0.25
0.5
1.0
$Ca^* = 8$
10^{-1}
1
10
10^2
Capillary Number, $Ca \equiv \frac{\mu_{nw} U L R_g}{\sigma K k_{rnw}}$

Figure 18

LAWRENCE BERKELEY LABORATORY
TECHNICAL INFORMATION DEPARTMENT
UNIVERSITY OF CALIFORNIA
BERKELEY, CALIFORNIA 94720